pH-dependent direct sulfhydrylation pathway is required for the pathogenesis of *Mycobacterium tuberculosis*

Vaibhav Kumar Nain[1,2], Vishawjeet Barik[1,2#], Manitosh Pandey[1#], Mohit Pareek[3], Taruna Sharma[1,2], Rahul Pal[1], Shaifali Tyagi[1], Manish Bajpai[4], Prabhanjan Dwivedi[5], Bhishma Narayan Panda[5], Yashwant Kumar[4], Shailendra Asthana[3] and Amit Kumar Pandey[1,5*]

[1]Mycobacterial Pathogenesis Laboratory, Centre for Tuberculosis Research, BRIC-Translational Health Science and Technology Institute, Haryana, India

[2]Special Centre for Molecular Medicine, Jawaharlal Nehru University, New Delhi, India

[3]Computational Biophysics and CADD Group, Computational and Mathematical Biology Centre, BRIC-Translational Health Science and Technology Institute, Haryana, India

[4]Biomarker Discovery Laboratory, Non-Communicable Diseases Centre, BRIC-Translational Health Science and Technology Institute, Haryana, India

[5]Experimental Animal Facility, BRIC-Translational Health Science and Technology Institute, Haryana, India

[#] Contributed equally to this work

*** Correspondence:** Amit Kumar Pandey, amitpandey@thsti.res.in

Abstract

Methionine is essential for the survival of *Mycobacterium tuberculosis* (*M. tuberculosis*) inside the host. However, the transsulfuration pathway, a major contributor of methionine, is dispensable for the growth of *M. tuberculosis* suggesting redundancy in the methionine biosynthesis pathway. Orthologues of $MetZ_{TB}$ in other bacterial species are known to operate a redundant single-step methionine

biosynthesis pathway called *direct sulfhydrylation.* In this study, we demonstrate that genetic disruption of the *metZ*-mediated direct sulfhydrylation pathway in *M. tuberculosis* hinders growth at low pH, an effect mitigated by methionine supplementation. Computational analyses, including *in-silico* molecular docking and molecular dynamics (MD) simulations, reveal enhanced binding of the MetZ substrate, O-succinyl homoserine (OSH), to the active site of MetZ at acidic pH. Intriguingly, despite increased intracellular ATP levels, a relative decrease in the frequency of Bedaquiline (BDQ)-induced persisters is observed in *metZ*-deficient strain, suggesting a role of direct sulfhydrylation pathway in modulating BDQ sensitivity. Finally, we demonstrated that the absence of *metZ* impedes the ability of *M. tuberculosis* to grow inside the host.

Keywords: tuberculosis, methionine biosynthesis, acidic pH, drug tolerance, transsulfuration, direct sulfhydrylation.

Introduction

Tuberculosis, an ancient disease, continues to pose a serious global health challenge, negatively impacting economies and the public health systems worldwide. In 2023, *Mycobacterium tuberculosis* (*M. tuberculosis*) caused 1.8 million deaths, making it the leading cause of death from a single infectious agent [1]. A steady increase in the frequency of drug-resistant tuberculosis cases has significantly complicated the therapeutic landscape. A majority of the approved drugs target pathways that are essential for the survival of *M. tuberculosis*. Targeting biosynthesis of essential amino acids as a therapeutic strategy has demonstrated immense potential and has yielded several molecules with the potential to become a future drug [2].

Methionine plays a pivotal role in cellular function, serving as the initiator amino acid, *N-formyl*-L-methionine (*f*Met), in protein synthesis in prokaryotes as well as protein degradation in eukaryotes [3]. Methionine also acts as a precursor for biosynthesis of essential metabolites that includes cysteine, biotin and SAM (S-adenosyl methionine). Given its critical importance, inhibiting some of the essential

47 proteins involved in the methionine biosynthesis pathway has been extensively investigated as a
48 potential strategy to identify new drugs against tuberculosis [4-8]. The transsulfuration pathway,
49 comprising a series of enzymatic reactions and intermediates involved in methionine biosynthesis, is
50 largely conserved across various microbial species and has been extensively reviewed [9]. Although
51 biosynthesis of methionine is known to be essential for the growth of *M. tuberculosis* [4, 6, 10], some
52 genes in this pathway are dispensable, indicating potential redundancy or conditional essentiality [11-
53 13]. Several reports suggest the existence of an alternate biochemical reaction in which the metabolite
54 O-succinyl homoserine (OSH) is directly converted into homocysteine [12, 14]. Interestingly, instead
55 of cysteine, host-generated hydrogen sulfide (H_2S) acts as the S-donor in this reaction catalyzed by the
56 enzyme O-succinyl homoserine sulfhydrylase (OSHS). The direct sulfhydrylation step allows several
57 microbial species to bypass the two-step conversion of OSH to homocysteine via cystathionine, a
58 crucial intermediate in the canonical methionine biosynthesis pathway [9, 15-17]. The presence of a
59 putative OSHS encoded by *metZ* (*Rv0391*) in *M. tuberculosis* suggests the existence of a yet
60 uncharacterized active direct sulfhydrylation pathway in *M. tuberculosis* [18].
61 In this study, employing genetic and computational approaches, we investigate the necessity of
62 redundant methionine biosynthesis pathways in *M. tuberculosis*. We demonstrate that *metZ* gene is
63 required for methionine biosynthesis under acidic conditions. Using computational approach, we
64 further demonstrate that the binding of the substrate to the active site of the enzyme MetZ is more
65 stable at acidic pH. Using CRISPR-mediated gene silencing, we provide evidence that *metZ*-dependent
66 direct sulfhydrylation pathway in *M tuberculosis* functions independently of the transsulfuration
67 pathway. The failure of *M. tuberculosis* strain, lacking both the transsulfuration and direct
68 sulfhydrylation pathways, to grow in methionine-lacking medium further validates the redundancy of
69 these pathways and suggests that the *metZ*-mediated direct sulfhydrylation pathway becomes
70 conditionally essential for the pathogen to survive under acidic and *in-vivo* growth conditions. In

71 conclusion, we report that *metZ*-mediated direct sulfhydrylation pathway is the primary driver of the
72 methionine biosynthesis under acidic conditions and is therefore essential for the survival of *M.*
73 *tuberculosis* within the host.

74 **Results**

75 **MetZ is dispensable for the *in-vitro* growth of *M. tuberculosis* and possibly involved in direct**
76 **sulfhydrylation pathway for methionine biosynthesis**

77 While *metZ* has been reported to be essential for the growth of *M. tuberculosis* on cholesterol [19], we
78 hypothesized that the *Rv0391 (metZ)* gene encodes a putative O-succinylhomoserine sulfhydrylase
79 (OSHS) that is responsible for direct sulfhydrylation (Fig. 1A). We performed a bioinformatics-based
80 analysis using the protein sequence of $MetZ_{TB}$ and found that the putative sequence belonged to the
81 cluster of orthologues group ENOG502GJ5S which is composed of 1097 protein sequences
82 orthologous to $MetZ_{TB}$ across 644 bacterial species. This cluster of proteins comprises various enzymes
83 involved in cellular amino acid metabolism namely, cysteine, methionine, homocysteine, serine and
84 aspartate. Co-incidently, all these proteins have a common PLP (pyridoxal-5-phosphate) – binding
85 domain which is essentially a modified lysine residue that covalently binds the co-factor, hence also
86 categorized as PLP-binding superfamily of proteins (Fig. 1B and S1A). Further, to elucidate the role
87 of *metZ* in *M. tuberculosis*, a deletion mutant in the genetic background of H37Rv (*Rv-WT*) was
88 generated by genetic recombineering as described previously [20]. Briefly, a hygromycin resistance
89 cassette was inserted into the ORF encoding *metZ* (*Rv0391*) with the help of allelic exchange substrate
90 (AES) consisting of 1kb regions of homology upstream and downstream to the target locus. The
91 recombinants were screened for hygromycin resistance and the cassette was subsequently excised out
92 thereby generating an unmarked mutant (Fig. 1C). The loss of the genetic sequence between 470034-
93 471188 bases was confirmed by gene-specific PCR (Fig. S2A), DNA sequencing of the locus (Fig.
94 S2B) and at the transcript level by RT-qPCR (Fig 1D). To check the essentiality of the *metZ* gene in

95 growth on cholesterol, we compared the growth of *Rv-WT*, *ΔmetZ* and the complement luminescence
96 reporter strains in different media containing glycerol (0.1%), cholesterol (200μM), propionate
97 (10mM) as the sole carbon source. As a control, we used the *M. tuberculosis* strain lacking the *prpR*
98 gene (*ΔprpR)* which is known to be essential for growth on cholesterol [21]. While, as expected, *ΔprpR*
99 failed to grow on cholesterol and propionate*,* the growth of all the three strains were comparable
100 irrespective to the carbon source (Figs. 1E, 1F and S3B). These findings indicate *metZ* does not
101 contribute to the central carbon metabolism and is dispensable for *in-vitro* growth of *M. tuberculosis*
102 on cholesterol and/ or propionate.

103 ***metZ* deletion renders *M. tuberculosis* sensitive to physiological stressors and leads to reduced *ex-***
104 ***vivo* fitness**

105 To replicate and grow inside the host, intracellular pathogens have evolved mechanisms to neutralize
106 the host-induced physiological stressors imposed by the host environment, including oxidative stress,
107 insult to the cell membrane, acidic pH and nutrient limitation. To study the role of *metZ* in mitigating
108 these host-induced stress, the *M. tuberculosis* strains were exposed to a range of stress-inducing
109 reagents. The effect of these stresses on each strain was subsequently assessed by calculating the
110 survival index relative to the *Rv-WT* strain. In comparison to the *Rv-WT* and complement strains,
111 *ΔmetZ,* demonstrated a reduced ability (~40-60%) to survive under all the stress conditions tested (Fig.
112 2A). Further, we determined intra-bacterial redox state using respective *M. tuberculosis* strains
113 expressing genetically encoded redox biosensor (Mrx1-roGFP2). To establish the dynamic range of
114 the biosensor readout, *Rv-WT* and the *ΔmetZ* strains expressing Mrx-roGFP2 were treated with H_2O_2
115 and Dithiothreitol (DTT) to achieve maximum oxidation and reduction states, respectively. This
116 defined the upper and lower limits of the biosensor response (dotted lines in Fig. 2B). We demonstrate
117 that in comparison to *Rv-WT*, the *ΔmetZ* strain exhibited significantly higher intracellular ROS levels

118 (Fig. 2B) suggesting an inability of the mutant to maintain redox homeostasis possibly due to impaired
119 mycothiol recycling. Notably, unlike *Rv-WT*, we did not observe any additional increase in
120 fluorescence signal in H_2O_2 treated *ΔmetZ* strain, further supporting the presence of elevated ROS
121 levels that may have saturated the biosensor (Fig. 2B). Subsequently, increased levels of lipid
122 hydroperoxides were detected in the *ΔmetZ,* strain compared to the *Rv-WT* and complement strains,
123 further corroborating our previous finding that the absence of *metZ* gene in *M. tuberculosis* results in
124 excessive accumulation of intracellular reactive oxygen species (Fig. 2C). Further, to assess the role of
125 *metZ* in the intracellular survival of the *M. tuberculosis* inside the macrophages, resting or IFN-γ
126 induced THP1-derived macrophages were infected with *Rv-WT*, *ΔmetZ* and the complement strains
127 and survival indices (w.r.t. *Rv-WT*) were determined by enumerating the bacterial load by CFU (Colony
128 Forming Unit) plating of the infected cell lysates at day 5 post-infection. We observed a significant
129 reduction in bacterial burden in the *ΔmetZ* strain compared to both *Rv-WT* and complement strains in
130 both resting (~60%) and activated (~48%) macrophages (Fig. 2D and S4A). Since restricting the
131 phagosome-lysosome fusion is a common strategy employed by the pathogen to enhance its
132 intracellular survival, we further investigated the role of *metZ* in regulating this process. Briefly, IFN-
133 γ induced THP1 macrophages infected with mEmerald (GFP) expressing *Rv-WT*, *ΔmetZ* and
134 complement strains were subsequently stained with Lysotracker. The study revealed that in comparison
135 to the *Rv-WT* and complement strains, the *ΔmetZ* strain exhibited a higher propensity to localize within
136 the acidic compartments of the cell (Fig. 2E and S5A). Overall, these data suggest that absence of *metZ*
137 significantly weakens the ability of *M. tuberculosis* to resist host-induced physiological stresses and
138 evade phago-lysosome fusion, both of which are crucial for the survival of the pathogen within the host
139 cell.

140 **Direct sulfhydrylation pathway is essential for *M. tuberculosis* to survive under low pH**

141 The observed data suggest that the *ΔmetZ* strain might exhibit increased sensitivity on exposure to an
142 acidic environment. To investigate this, we cultured different bacterial strains (*Rv-WT*, *ΔmetZ* and
143 complement) at varying pH values and monitored their growth kinetics. While the growth kinetics were
144 comparable at neutral pH (7.2) for all the strains, a decrease in pH resulted in a discernible growth
145 defect in the *ΔmetZ* strain, ranging from observable impairment at pH 5.5 to complete growth arrest at
146 pH 5.0, relative to the *Rv-WT* and complement strain (Fig. 3A and S6A and B). To further understand
147 the impact of acidic pH on the expression of genes involved in transsulfuration (*metB* and *metC*) and
148 direct sulfhydrylation (*metZ*), we quantified the relative expression of these genes in *M. tuberculosis*
149 cultured at pH 7.2 and pH 5.5. RT-qPCR analysis revealed an ~12-fold increase in the expression of
150 *metZ* gene at pH 5.5 compared to pH 7.2, suggesting transcriptional induction of the *metZ* gene under
151 acidic conditions (Fig. 3B). To differentiate between bacterial killing and metabolic slowdown as the
152 cause of reduced CFU counts in the *ΔmetZ* strain at pH 5.5 (Fig. S6C), we assessed metabolic activity
153 using Resazurin dye [22]. We found that, in contrast to the *Rv-WT* and complement strains, the *ΔmetZ*
154 strain exhibited significantly reduced metabolic activity at pH 5.5, as indicated by lack of color change
155 and low fluorescence, suggesting a significant impairment in metabolic function (Fig. 3C).
156 Surprisingly, despite this metabolic impairment, ATP levels in the *ΔmetZ* strain were found to be higher
157 than those in the *Rv-WT* and complement strains when cultured at acidic pH 5.5 (Fig. 3D).

158 Given that the first-line anti-TB drug - Pyrazinamide (PZA) is active only at acidic pH and efficiently
159 kills slow or non-replicating cells, we hypothesized that the differences in the cytoplasmic pH will
160 correlate with PZA sensitivity. As expected, we observed a ~19-fold and 4-fold increase in the
161 sensitivity of the *ΔmetZ* strain to PZA treatment compared to *Rv-WT* and complement strain,
162 respectively (Fig. 3E). To confirm, if the observed phenotype is a direct consequence of a defect in the
163 methionine biosynthesis, we quantified the intracellular methionine levels. We found significantly
164 lower levels of methionine in both *Rv-WT* and *ΔmetZ* strains grown in acidic pH 5.5 compared to those

165 grown at pH 7.2 (Fig. 3F). Exogenous supplementation of methionine rescued the growth defect
166 phenotype of *ΔmetZ* observed at pH 5.5 (Fig. 3G). Importantly, the addition of methionine did not alter
167 the pH of the culture media (Fig. S6D and E). Furthermore, we observed a reduction in the intracellular
168 ROS levels in *ΔmetZ* upon exogenous supply of methionine at pH 7.2 while this effect was less
169 pronounced at pH 5.5 (Fig 3H). Concurrently, methionine supplementation not only restored ATP
170 levels but also increased the IC50 of PZA in the *ΔmetZ* at pH 5.5 (Fig 3I and S6F). *M. tuberculosis*
171 produced significantly higher levels of hydrogen sulfide (H_2S) at acidic pH compared to the neutral pH
172 (Fig S6G). H_2S serves as a co-substrate and S-donor in the reaction catalyzed by OSHS enzyme (MetZ),
173 an enzyme belonging to the PLP-dependent superfamily of proteins which require PLP as co-factor
174 (Fig 1B and S1). To assess the role of *metZ* in PLP homeostasis, we examined the growth kinetics of
175 different mycobacterial strains in minimal medium supplemented with or without PLP at both pH 7.2
176 and pH 5.5. We found that knocking out *metZ* had no apparent consequences on the growth kinetics of
177 the *M. tuberculosis* with or without PLP at either pH conditions (Fig. S7A and B). However, we did
178 observe a low pH-based growth defect in *ΔmetZ* even in minimal medium (Fig. S7B). In summary, a
179 defect in the methionine biosynthesis pathway at low pH renders the *ΔmetZ* strain metabolically less
180 active, thereby inhibiting its growth at acidic pH.

181 **Molecular docking and Molecular dynamics (MD) simulations revealed enhanced stability of**
182 **MetZ at acidic pH**

183 To investigate the molecular mechanisms underlying MetZ substrate binding and their kinetics at
184 physiologically relevant pH (7.0 and 5.4), we employed computational approaches, including
185 molecular docking and molecular dynamics simulations studies. To perform *in-silico* molecular
186 docking with MetZ protein (Fig. 4A), we determined the binding site of O-succinyl homoserine (OSH)
187 by focused molecular docking [23, 24] that provided the final pose at the cofactor bound site. A pose

188 with docking energy of -4.07 Kcal/mol and cluster size of 50 (out of 200) was found suitable at pH 7.0.
189 While, at pH 5.5 the most likely pose showcased a docking energy of -4.19 Kcal/mol with a cluster
190 size of 80 (200). For both these poses at diverse pH, a static thermodynamic quantification was carried
191 out using MM-GBSA which was found to be -49.20 Kcal/mol and -56.93 Kcal/mol, respectively.
192 Molecular Dynamics Simulation at a constant pH was performed for these poses. Following the 300ns
193 MD simulations, the protein exhibited stable RMSD values at 2.98 Å and 4.34 Å at pH 7.0 and 5.5,
194 respectively. However, significant changes were observed in the stability of the substrate as well as the
195 occupied binding site. On observing the substrate in consensus with its binding site, the region was
196 found to have higher stability and an average RMSD of 1.87 Å was observed at pH 5.5 in comparison
197 to an average of 2.71 Å at pH 7.0 (as shown in Fig. 4B and D). The underlying reason for this higher
198 stability at pH 5.5 is due to the establishment of stable durable bonds in the form of hydrogen bonds
199 with residues V196, F197 and T319 and the O-atoms at the terminals of the substrate. Furthermore,
200 another factor which enhances the strength is the formation of a salt-bridge with residue H220 and
201 substrate. However, a similar configuration of H-bonds and salt-bridge are not observed at pH 7.0,
202 possibly due to conformational dynamics [25] (Fig. 4E). These characteristics are a result of the change
203 in pKa values as well as conformations of the binding site forming amino acid residues. Protonation
204 states of amino acids are highly susceptible to change in environmental pH and thus, preparing the
205 protein at pH 7.0 and 5.5 generates different acid dissociation constants, which ultimately affects the
206 bond forming tendencies of residues. The residue E165 attains a pKa of 8.78 at pH 7.0 and donates a
207 proton, forming a bond with the substrate. Similarly, D194 attains a pKa of 9.11 at pH 5.5 which affects
208 its binding to the substrate. Also, H220 is present in a protonated state at a lower pH and thus involved
209 in the formation of a Salt-Bridge with the substrate. While at pH 7.0, H220 remains in a deprotonated
210 state and thus does not contribute to the stability of the binding pocket at neutral pH. This showcases
211 the importance of the acidic pH which contributes to relatively greater stability of the substrate. On

212 analysis of the binding site, we found that H220 and T319 interact with the substrate at the acidic pH
213 but they showcase conformational changes at pH 7.0 which hinders their interaction. The imidazole
214 ring sidechain of H220 rotates in anti-clockwise direction and thus does not get involved in bond
215 formation. Similarly, T319 forms H-bonds at both pH but the nature of the bonds varies from transient
216 at pH 7.0 to largely consistent at pH 5.5. Overall, conformational changes in the binding site residues
217 can be accredited for better stability at pH 5.5 The stability of the protein and the substrate at acidic
218 pH hints towards a better binding activity of the substrate. This characteristic feature can be examined
219 by performing the MM-GBSA of a few selected frames from both the trajectories to compare their
220 activity. The average binding/biological activity of the protein is found to be -37.35 Kcal/mol and -
221 59.40 Kcal/mol at pH 7.0 and 5.5, respectively (Fig. 4C). This increase in the binding affinity is due to
222 the effect of acidic pH on the protonation state as well as the induced conformational changes. The
223 docking scores at both pH 7.0 & 5.5 suggest that the residence time of the substrate at the binding site
224 must be short and the sulfur transfer reaction might be transient. Overall, focused docking and MD
225 simulations revealed that although protein is stable at both acidic and neutral pH, the active site of the
226 protein holds substrate (OSH) more stably at acidic pH rather than at neutral pH which sheds light on
227 its physiological role in methionine biosynthesis at acidic pH instead of neutral pH in concordance
228 with our *in-vitro* studies.

229 ***metZ*-mediated direct sulfhydrylation pathway is critical for methionine biosynthesis at acidic**
230 **pH**

231 To investigate the independence of the *metZ*-dependent methionine biosynthesis pathway from the
232 transsulfuration pathway in *M. tuberculosis*, we employed CRISPRi to knockdown *metB* (*Rv1079*)
233 expression in both *Rv-WT* (*Rv::metB*$_{KD}$) and *ΔmetZ* (*ΔZ::metB*$_{KD}$) strains (Fig. 5A).
234 Anhydrotetracycline (ATc)-induced knockdown of *metB* expression in both strains was confirmed by

235 RT-qPCR analysis (Fig. S8A). While ATc-induced knockdown of *metB* had no significant effect on
236 the growth of the *Rv-WT* strain, it resulted in a growth defect in the *ΔZ::metB*$_{KD}$ strain, effectively
237 mimicking a double knockout phenotype (Fig. 5B and S8B). This growth defect is likely attributed to
238 a compromised methionine biosynthesis pathway, as evidenced by a ~1.5-fold decrease in the
239 intracellular methionine levels in the *ΔZ::metB*$_{KD}$ strain compared to the *Rv::metB*$_{KD}$ strain (Fig. 5C).
240 Based on these findings we hypothesized that the *ΔZ::metB*$_{KD}$ double mutant would exhibit attenuated
241 growth in an animal model due to reduced methionine availability. To test this hypothesis, mice were
242 infected with *Rv::NT* (Non-targeting control sgRNA) and *ΔZ::metB*$_{KD}$ strains, and doxycycline was
243 administered to the specific groups to induce CRISPRi-mediated knockdown of the respective gene.
244 Bacterial load was subsequently estimated by CFU plating (Fig 5D). We found that compared to NT
245 and *ΔmetZ*, the *ΔZ::metB*$_{KD}$ double mutant exhibited reduced bacterial burden during the initial stages
246 of infection in both lungs and spleen which was partially rescued by week 6 post infection (Fig. 5E).
247 We hypothesized that the presence of an active methionine transporter, such as MetM (Rv3253c) [26]
248 might contribute to the partial rescue of the growth defect observed in the animal infected with
249 *ΔZ::metB*$_{KD}$ double mutant strain of *M tuberculosis*. Collectively, the above data demonstrate the
250 functional independence of the MetZ-mediated direct sulfhydrylation pathway in *M. tuberculosis.* The
251 observed growth defects and reduced methionine levels in the *ΔZ::metB*$_{KD}$ strain both *in-vitro* and *in-*
252 *vivo* models highlight the critical role of these redundant pathways in supporting bacterial growth and
253 survival inside the host.

254

255 **Direct sulfhydrylation pathway of *M. tuberculosis* contributes towards antibiotic persistence in**
256 **response to Bedaquiline**

257 Next, we wanted to study the role of direct sulfhydrylation pathway in regulating the drug susceptibility
258 profile of *M. tuberculosis*. We first compared the Minimum Inhibitory Concentration (MIC) of various
259 anti-TB drugs. We found that the IC50 values for each of these drugs were similar for all three strains
260 (*Rv-WT*, *ΔmetZ* and the complement strain) (Fig. 6A and 9A-D, F). Further, a time-kill assay was
261 performed to determine the role of *metZ* in modulating the formation of drug-induced persisters in *M.*
262 *tuberculosis*. The frequency of persisters formation was assessed by comparing the biphasic kill curves
263 generated from the time-kill assays using various antibiotics (RIF, INH, EMB and BDQ) at 10X MIC
264 concentrations. No significant differences in the persisters formation were observed among the strains
265 when treated with RIF, INH or EMB (Fig. 6B). Interestingly, compared to the *Rv-WT* and the
266 complement strains, a significant decrease in the persisters formation was observed in the *ΔmetZ* upon
267 treatment with BDQ at both neutral (Fig. 6B) and acidic pH (Fig. S9E). While a biphasic kill curve
268 was observed for the *ΔmetZ* treated with BDQ at pH 7.2, the kill curve at pH 5.5 was predominantly
269 linear, suggesting a lower frequency of persisters formation at acidic pH. Given BDQ inhibits ATP
270 synthesis, we hypothesized that the observed decrease in the persisters formation in the *ΔmetZ* might
271 be due to impaired generation of ATP. However, ATP depletion kinetics analysis using 2X MIC BDQ
272 revealed higher ATP levels in the *ΔmetZ* compared to the *Rv-WT* and the complement strains (Fig. 6C),
273 suggesting that BDQ-mediated ATP depletion was slower in the *ΔmetZ* strain. In sum, we found that
274 the *metZ*-mediated direct sulfhydrylation pathway modulates the susceptibility of *M. tuberculosis* to
275 BDQ and that the reduction in the BDQ-dependent persisters generation observed in the *M.*
276 *tuberculosis* strain lacking *metZ* is independent of the ATP levels present inside the bacteria.

277 **Direct sulfhydrylation pathway supports the growth of *M. tuberculosis* inside the host**

278 To elucidate the role of *metZ* in mycobacterial pathogenesis, a guinea pig model of tuberculosis
279 infection was employed. Briefly, guinea pigs were infected with the respective mycobacterial strains

280 (*Rv-WT*, *ΔmetZ* and complement) via the aerosol route. Bacterial burden in the lungs and the spleen
281 was determined by CFU plating at different time points post-infection. Gross and histopathological
282 analyses were performed to study the damage due to infection at the tissue level (Fig. 7A). We found
283 that at week 4 post-infection the bacterial burden in the lungs of guinea pigs infected with *ΔmetZ* was
284 significantly lower than that observed in animal infected with the *Rv-WT* and complement strains,
285 exhibiting a ~3.7-fold and 2-fold reduction, respectively. By 8 weeks post-infection, a more
286 pronounced difference was observed, with approximately an 8.9-fold reduction in the bacterial burden
287 in the lungs of *ΔmetZ*-infected animals compared to those infected with the *Rv-WT* strain. Notably,
288 only a modest increase in CFU counts was observed in the *ΔmetZ*-infected animals between weeks 4
289 and 8 (Fig. 7B). Similarly, a 6-fold reduction in bacterial burden was observed in the spleens of animals
290 infected with the *ΔmetZ* compared to those infected with the WT and complement strains at week 4
291 post-infection. By week 8, bacterial burden in the spleens of the *ΔmetZ*-infected animals was
292 significantly reduced, approaching the limit of detection by CFU and exhibiting a nearly 263-fold
293 decrease compared to week 4 post-infection (Fig. 7C). Consistent with the reduced bacterial burden
294 (Fig. 7B), gross pathology revealed fewer granulomatous lesions in the lungs of animal infected with
295 the *ΔmetZ* compared to those infected with the *Rv-WT* and complement strains at 8 weeks post-infection
296 (Fig. 7D). To visualize and quantify the damage to lung tissues, Hematoxylin & Eosin (H&E) staining
297 of the formalin preserved lung sections was done. Microscopic examination of lung samples collected
298 from animals infected with *Rv-WT* strain revealed severe granulomatous inflammation throughout the
299 lung parenchyma. Numerous well-defined necrotizing granulomas consisting of epithelioid histiocytes,
300 perimetric cuffing of lymphocytes and plasma cell aggregates and a caseous necrotic mass at the centre
301 were observed. However, lung samples from animals infected with complement strain and *ΔmetZ* strain
302 showed only non-necrotizing granulomas along with multiple foci of inflammatory cell aggregates and
303 occasional alveolar hemorrhagic patches (Fig. 7E). Granuloma scoring further confirmed these

304 observations, with the highest scores observed in lungs sections from animals infected with the *Rv-WT*
305 strain, followed by those infected with the complement and *ΔmetZ* strains (Fig. 7F). Overall, these data
306 suggests that absence of *metZ* gene significantly impairs the ability of *M. tuberculosis* to replicate and
307 survive within the host, suggesting that the *metZ*-dependent direct sulfhydrylation pathway is crucial
308 for the survival of the pathogen inside the host.

309 ***metZ* is involved in methionine biosynthesis in *M. tuberculosis* at acidic pH**

310 We hereby summarize that upon infecting macrophages, *M. tuberculosis* traverses a series of
311 intracellular compartments, initially residing in the phagosomes where a relatively neutral pH (~6.5)
312 and abundant nutrients, including methionine that support bacterial growth. However, as host immunity
313 mounts, IFN-γ-mediated induction of reactive oxygen species (ROS) and reactive nitrogen
314 intermediates (RNI) triggers phagosomal maturation leading to a severe drop in the pH (5.5 or lower).
315 These acidic conditions, coupled with nutrient restrictions imposed by the host, create a hostile
316 environment that inhibits the growth of the pathogen. In response to these stressors, *M. tuberculosis*
317 undergoes substantial transcriptional and metabolic reprogramming. One critical adaptation involves
318 the induction of *metZ* expression, which enables the pathogen to survive these challenging conditions.
319 The MetZ-mediated direct sulfhydrylation pathway utilizes host-derived H_2S as a co-substrate and S-
320 donor for methionine biosynthesis within this acidic microenvironment, facilitating the maintenance
321 of ATP levels, mycothiol recycling and overall metabolic activity (Fig. 8).

322

323 **Discussion**

324 *M. tuberculosis*, adapts to various hostile conditions within host macrophages resulting in the
325 differential expression of proteins crucial for its survival. One such key adaptation involves increase in
326 the biosynthesis of cysteine which compensates for the increase in the flux of cysteine towards

327 generating the thiol-active metabolites (mycothiol, ergothioneine, NAD+, etc.). These metabolites are
328 essential for maintaining the redox balance upon exposure to heightened levels of ROS, RNI [27] and
329 acidic pH [28]. The same has been reported in *E. coli*, where increased oxidative stress leads to higher
330 demand for the cytosolic glutathione which stimulates cysteine biosynthesis [29]. Under such
331 demanding circumstances, the pathogen needs to evolve and devise a mechanism to efficiently regulate
332 the flux of cysteine towards either biosynthesis of methionine and/or mycothiol which would maintain
333 the total thiol pool thereby maintaining redox homeostasis. Likewise, given the crucial role of
334 methionine in bacterial physiology, there has been a gap in our understanding of the rationale of
335 harbouring multiple methionine biosynthesis pathways and their role in maintaining methionine
336 homeostasis critical for the survival of *M. tuberculosis* in a nutrient-deprived *in-vivo* growth
337 environment. We, in the current study, have used a combination of genetics and computational biology-
338 based tools to probe the role of the *metZ*-mediated direct sulfhydrylation pathway in *M. tuberculosis*.
339 We found that MetZ-dependent direct sulfhydrylation is significantly induced at acidic pH. Disrupting
340 this pathway in *M. tuberculosis* results in a decrease, but not complete elimination, of cellular
341 methionine at low pH. Finally, we demonstrated that MetZ-dependent direct sulfhydrylation is required
342 for growth of *M. tuberculosis* inside the host.

343 In contrast to an earlier report [19], *metZ* was found to be dispensable for the growth of *M. tuberculosis*
344 on cholesterol. The conditional essentiality phenotype observed for *ΔmetZ* under low pH further
345 suggests that the earlier observation of the *metZ* essentiality on cholesterol likely resulted from the low
346 pH growth conditions used in that study. High demand for cysteine, a common precursor for the
347 generation of both methionine and mycothiol, during stress resulted in observed imbalance in the redox
348 homeostasis in *ΔmetZ*. Exogenous supplementation of methionine alleviates the stress by reducing the
349 need to divert the intracellular cysteine pool towards methionine production, thereby enhancing the
350 mycothiol generation critical for mitigating the ROS levels at acidic pH. Beyond redox homeostasis,

351 our data underscores the role of methionine biosynthesis, through the direct sulfhydrylation pathway,
352 in regulating the cytosolic pH and metabolism. The inability of the *ΔmetZ* to maintain the intracellular
353 pH homeostasis impedes the ability of the pathogen to utilize the cellular ATP, leading to a metabolic
354 slowdown. The elevated levels of ATP observed in *ΔmetZ* at acidic pH, is likely, a consequence of
355 reduced ATP utilization rather than overproduction as reported in an earlier study using *E. coli* [30].

356 The enhanced susceptibility of *ΔmetZ* to Pyrazinamide (PZA), an anti-TB prodrug that gets activated
357 upon exposure to acidic pH, further confirms the presence of a relatively acidic cytosol and accentuates
358 the role of *metZ* in maintaining the pH homeostasis in *M. tuberculosis*. In an *ex-vivo* setting, IFN-γ-
359 induced activation leads to acidification of the pathogen containing phagosomes in macrophages.
360 Consequently, *ΔmetZ* replication inside both resting and the activated macrophages were reduced,
361 likely due to increased co-localization of *ΔmetZ* to acidic compartments as revealed by confocal
362 microscopy. This finding aligns with previous studies suggesting that enhanced susceptibility to
363 oxidative stress results in increased bacterial killing in the acidified macrophage compartments [31-
364 33].

365 Our data provides a mechanistic understanding of the methionine starvation-associated susceptibility
366 in *M. tuberculosis* in line with reports published by other groups [4, 10]. The presence of both
367 transsulfuration and direct sulfhydrylation pathways for the biosynthesis of methionine in *M*
368 *tuberculosis* is indeed intriguing. Although both the pathways demonstrate redundancy at normal pH,
369 our qPCR data, along with previous studies, categorically indicate that enzyme responsible for carrying
370 out direct sulfhydrylation is over-expressed in *M tuberculosis* upon induction with acidic pH [32, 34,
371 35]. These findings are corroborating well with our pH dependent molecular dynamics (MD)
372 simulation studies which suggested that the binding affinity between the substrate and MetZ active site
373 is stronger at low pH. The MD simulation data provide structural insights into how pH and the
374 protonation states of key residues alter the hydrogen bonding and electrostatic interaction network

375 leading to significant changes in the conformation of the MetZ protein. The change in the hydrogen
376 bonding network, identified as a determinant, majorly impacts the change in the binding affinity of the
377 substrate. Furthermore, a comparative analysis of MetZ structural stability at different pH values, using
378 metrics such as root-mean-square deviation (RMSD) and thermodynamic changes, confirms the pH-
379 dependent behaviour of MetZ. The observed changes in the hydrogen bonding network significantly
380 impact the substrate binding affinity of the MetZ, indicating that, under low pH conditions, *metZ*-
381 mediated direct sulfhydrylation majorly contributes towards the biosynthesis of methionine in *M.*
382 *tuberculosis*. We further confirm that *M. tuberculosis* strain that lacks both transsulfuration and direct
383 sulfhydrylation pathways (*ΔmetZ/metB*$_{KD}$) fails to generate methionine, demonstrating methionine
384 auxotrophy under *in-vitro* conditions. This finding confirms the redundancy that exists between these
385 two pathways. Surprisingly, the growth defect observed in the *ΔZ::metB*$_{KD}$ under *in-vivo* conditions,
386 while significant, was less pronounced than that observed *in-vitro*. This may be attributed to the
387 presence of a potential methionine transporter, encoded by Rv3253c (MetM), which allows the
388 pathogen to salvage methionine from the host environment [26]. Similar to our finding (Fig. S6G), it
389 has been reported previously that *M. tuberculosis* can produce H_2S, a gaseous signalling molecule,
390 upon induction with acidic pH [13] probably as a mechanism to counteract increasing ROS and
391 dropping metabolic potential of the cells. Further, it has also been shown that H_2S at sub-inhibitory
392 levels in *M. tuberculosis* have a positive effect on the mycobacterial electron transport chain (ETC)
393 and this effect is reversible [36, 37]. Additionally, host-generated H_2S has been shown to enhance *M.*
394 *tuberculosis* replication inside the host. This effect is evident in studies demonstrating impaired *M.*
395 *tuberculosis* replication when the hosts' ability to generate H_2S is compromised, either through genetic
396 knockout of the genes encoding the enzyme cystathionine-γ-lyase (CSE) and cystathionine-β-synthase
397 (CBS) or by using pharmacological inhibitors of these enzymes [36, 38, 39]. Co-incidentally, it is well

398 established in the literature that sulfhydrylases, including MetZ, utilize H_2S as a S-donor for various
399 reactions, such as cysteine biosynthesis or, in this case of MetZ, for the production of homocysteine.

400 The development of antibiotic persistence in bacteria is a significant contributor to the failure of anti-
401 TB treatment. The frequency of generation of the persisters population can be quantified through a
402 time-kill assay using high antibiotic concentration (5-10X MIC) [40]. Our time-kill experiments
403 suggest that the absence of a direct sulfhydrylation pathway in *ΔmetZ* prevents the BDQ-specific
404 generation of antibiotic persistence in *M. tuberculosis*. Intriguingly, despite exhibiting higher cytosolic
405 ATP levels compared to the wild-type strains, *ΔmetZ* demonstrated a decrease in the BDQ-mediated
406 persisters formation. This observation contrast with a previous study on *ΔpckA* mutant, wherein
407 elevated cytosolic ATP levels increased drug tolerance when grown in acetate medium [41]. In
408 summary, our findings suggest that beyond its role in maintaining methionine levels at acidic pH, the
409 direct sulfhydrylation pathway also modulates the generation of BDQ-specific generation of antibiotic
410 persistence during infection. Further investigation into this complex phenotype will be crucial for
411 developing new strategies to prevent the emergence of BDQ resistance in tuberculosis. Furthermore,
412 we found that *metZ* is essential for the maintenance of *M. tuberculosis* infection in guinea pig model,
413 as evident by a reduced bacterial burden and severe attenuation in the spleen. Spleen is known to be
414 iron rich, which can contribute to the generation of reactive oxygen species via Fenton chemistry.
415 Given the observed susceptibility of the *ΔmetZ* to oxidative stress, the low bacterial count in the spleen
416 at week 8 post-infection likely reflects the inability of the mutant to survive in this nutrient-deprived,
417 low pH and oxidative stress-inducing environment within the host. Our results indicate that *M.*
418 *tuberculosis* adapts to the decreasing pH in its surroundings by maintaining methionine biosynthesis
419 through direct sulfhydrylation utilizing exogenous and endogenous H_2S as S-donor.

420 This study provides a foundation for designing novel anti-tuberculosis treatment strategies. Using
421 pharmacological inhibitors of MetZ as an adjunct to the existing anti-tuberculosis regimens could offer

422 a promising approach. This synergistic strategy can potentially enhance the efficacy of the existing
423 treatment regimen against tuberculosis.

424

425 Materials and Methods

426 **Bacterial strains**

427 The knockout strain of *metZ* gene *(Rv0391)* was generated in the genetic background of wild type
428 *M. tuberculosis* H37Rv by genetic recombineering. Briefly, a gene-specific allelic exchange substrate
429 (AES) harboring 1kb sequences of target gene upstream and downstream homology flanking
430 Hygromycin resistance gene cassette was constructed in the suicidal vector pJM1. AES was
431 transformed into H37Rv (wild-type, *Rv*-WT) strain overexpressing Phage Che9c RecET proteins to
432 facilitate recombination. Recombinants with the Hygromycin resistance (Hyg^r) gene were selected
433 over Hygromycin (Hyg) plates and screened using gene-specific PCR. The marked mutant thus
434 prepared was unmarked to excise out Hygromycin resistance cassette using Cre-recombinase
435 expressed from plasmid pCre-SacB-Zeo. The unmarked mutant was confirmed by PCR and RT-
436 qPCR to confirm the loss of gene as well as transcripts of *metZ* gene. The unmarked mutant was then
437 transformed with a plasmid expressing a functional copy of the *metZ* gene under P_{myc1}*tetO* promoter
438 replicating either episomally or integrated to generate genetic complementation strain (denoted as
439 *ΔmetZ Comp*). Bioluminescent mycobacterial strains were generated by transforming respective
440 mycobacterial strains (**Table S3, List of strains used in the study**) with integrative plasmid
441 expressing *luxABCDE* operon (Addgene# 26161) [42] with slight modifications [43]. Strains were
442 checked for bioluminescence and a luminescence vs CFU plot was prepared with *Rv-WT*
443 luminescence reporter strain to determine the relation between luminescence and CFU-based read-
444 outs of bacterial viability (Fig. S3A). Henceforth, where ever appropriate, luminescence was used as
445 proxy for the bacterial viability and growth.

446

447 **Media and cultural conditions**

448 The bacterial strains were maintained as frozen glycerol stocks at -80°C. Whenever required, the stocks
449 were thawed and diluted 1:500 in 7H9 (Difco, BBL) medium supplemented with Oleic acid, Albumin,
450 Dextrose, Salt (NaCl) (OADS) and 0.01% Tween 80. Bacterial enumeration was done on 7H11 (Difco
451 BBL) agar plates supplemented with OADS. Kanamycin (Sigma), 25µg/ml, Hygromycin (Sigma),
452 50µg/ml and Zeocin (Invitrogen), 25µg/ml were used whenever required. For media with no carbon
453 source, 7H9 base medium was prepared without glycerol and OADS (or Albumin, Dextrose, Salt:
454 ADS) enrichment and later supplemented with desired Carbon (C)-sources and 0.05% tyloxapol.
455 100mM stock of Cholesterol (Sigma) was prepared by heating cholesterol in Tyloxapol (Sigma):
456 Ethanol (Merck) mix (1:4) at 80°C for 30 mins [44]. When required, cholesterol was diluted to desired
457 concentration (200µM) in 7H9 base medium wherever specified. Likewise, glycerol (Sigma) was used
458 at a final concentration 0.1% v/v and sodium propionate (Sigma) was used at a concentration of 10mM
459 (0.1%) for growth kinetics studies. For pH-dependent growth kinetics experiments, 7H9 base medium
460 was prepared, supplemented with 0.1% glycerol (v/v) and ADS acidified to desired pH using HCl. For
461 Pyridoxal-5'-Phosphate (PLP) supplementation-based growth kinetics, minimal medium (0.5g/litre
462 asparagine, 1g/litre KH_2PO_4, 2.5g/litre Na_2HPO_4, 50mg/litre ferric ammonium citrate, 0.5g/litre
463 $MgSO_4.7H_2O$, 0.5mg/litre $CaCl_2$, and 0.1mg/litre $ZnSO_4$) containing 0.1% glycerol (vol/vol) was used
464 with or without 50µg/ml PLP (Sigma) supplementation. Phosphate buffered saline (PBS) was used at
465 1X concentration supplemented with tyloxapol (0.05%), PBST whenever mentioned. Bacterial
466 enumeration by CFU was done on 7H11 agar plates supplemented with OADS, wherever mentioned.
467 Colonies were counted after 21 days of incubation. Anhydrotetracycline, ATc (Caymen) was used at
468 200-300ng/mL concentration unless mentioned otherwise. L-methionine (Sigma) was supplemented at
469 100µg/ml concentration wherever required.

470

471 **CRISPRi knockdown**

472 For transcriptional knockdown of *metB (Rv1079)* using CRISPR interference (CRISPRi), target-
473 specific sgRNA was cloned into *BsmBI* (NEB) digested backbone plJR965 (Addgene # 115163) to
474 generate knockdown construct. The knockdown construct was transformed into *Rv-WT* and *ΔmetZ*
475 strains through electroporation. To achieve knockdown of the target genes, cells were grown to mid-
476 log phase and diluted back to OD 0.01 in fresh culture medium with or without ATc. Growth was
477 monitored by measuring OD of the cultures. Further, expression of target genes was quantified by
478 qPCR to determine the levels of knockdown.

479

480 **RT-qPCR**

481 Total RNA was isolated from the respective bacterial strains under specific conditions using Trizol
482 (TaKaRa) according to the manufacturer's protocol. Briefly, bacterial cells were washed with 1X
483 PBS and resuspended in Trizol. Cells were lysed by bead-beating using 0.22µM sized zirconia beads
484 via 5 cycles with intermittent cooling step of 1 minute. Further, RNA was extracted and precipitated
485 using chloroform-isopropanol treatments. Total RNA thus prepared was treated with Turbo DNaseI
486 (Ambion) to digest away the DNA contamination. 3000 µg equivalent DNase treated RNA was
487 used to prepare cDNA using SuperScript IV Reverse Transcriptase (Invitrogen). Finally, 1µg
488 equivalent cDNA was used to set up qPCR reactions with SYBR (TaKaRa). *sigA* was used as
489 internal control and $\Delta\Delta C_t$ method [45] was used determine relative gene expressions w.r.t. specified
490 control conditions. For qPCR at acidic pH, *icl1* was used as positive control.

491

492 **Growth kinetics**

493 Auto-bioluminesc ent bacterial strains were grown till OD 0.5 (mid-log phase) and washed once
494 with 1X PBST to remove the spent media. The cells were resuspended in 1X PBST and diluted back
495 to an OD of 0.01 in 7H9 base medium supplemented with different carbon sources – glycerol
496 (0.1%), cholesterol (200µM) or propionate (10mM) for C-source dependent growth kinetics. For
497 pH-dependent growth kinetics, bacterial cells were diluted back to an initial OD of 0.05 in 7H9
498 medium (supplemented with ADS and 0.2% glycerol) acidified to different pH – 7.2, 6.5, 5.5 and
499 5.0. Whenever required, L-methionine (100µg/ml, Sigma) was added to the cultures and 50µg/ml
500 L-methionine was replenished every 4 days until the conclusion of the experiment. For CRISPRi
501 based growth kinetics, Anhydrotetracycline chloride (ATc) was added to the cultures (200ng/ml)
502 and replenished every 4 days to maintain the suppression of the target gene until the conclusion of
503 experiment. The growth was monitored by measuring OD and/ or auto-bioluminescence using a
504 Multimode Microplate reader (SpectraMax Pro ID3, Molecular Devices). At times, bacterial growth
505 was also determined by CFU at indicated time points by plating aliquots of cultures and plating
506 appropriate dilutions on 7H11 agar plates.
507
508 **Physiological stress survival assay**
509 Bacterial strains were grown till OD 0.5 (mid-log phase) and washed once with 1x PBST. Aliquots
510 of 2ml cell suspensions equivalent to OD 0.2 were treated with 0.5mM H_2O_2 (oxidative stress),
511 200µM Deta-NO (nitrosative stress), 0.01% SDS (membrane stress), PBST (nutrient starvation
512 stress), Phosphate citrate buffer, pH 5.5 (acidic stress) *in-vitro*. The survival of the respective strains
513 was determined by CFU plating at indicated time points and calculating survival index (i.e., CFU
514 of strain/ CFU of *Rv-WT*).
515
516 **Drug susceptibility (MIC determination)**

517 Auto-bioluminescent bacterial strains were grown till OD 0.5 (mid-log phase) and washed with 1x
518 PBST. Anti-TB drugs: Rifampicin (RIF), Isoniazid (INH), Bedaquiline (BDQ), Ethambutol (EMB),
519 Clofazimine (CFZ) and Pyrazinamide (PZA) were serially diluted on a 10-points, 2-fold format and
520 added to the 96-well plates (Corning). Cells were added at final density of OD 0.01 to the wells
521 containing drugs and incubated at 37°C for 3 days as described previously [46]. Finally,
522 luminescence was recorded as an indicator of bacterial viability which was expressed as dose-
523 response curves and IC_{50} were calculated using non-linear regression analysis in GraphPad Prism.
524 For MIC determination at pH 5.5, the drug dilutions and the bacterial suspensions (final density of
525 OD 0.05) were prepared in 7H9 medium supplemented ADS (pH adjusted to 5.5). For MIC
526 determination of PZA at pH 5.5 upon supplementation with methionine, an additional group of
527 *ΔmetZ* + Methionine was maintained. Dose-response curves were prepared similarly as described
528 above.
529
530 **Kill kinetics**
531 Bacterial strains were grown till OD 0.5 (mid-log phase) and washed with 1x PBST. Aliquots of
532 cell suspensions (2ml) at a bacterial density of OD 0.2 were treated with 10X MIC concentrations
533 of anti-TB drugs- Rifampicin (RIF), Isoniazid (INH), Ethambutol (EMB) and Bedaquilline (BDQ)
534 for mentioned time intervals. Bacterial survival was determined by CFU enumeration at indicated
535 time points. For pH-dependent kill kinetics of BDQ, 7H9 (+ADS) medium acidified to pH 5.5 was
536 employed and 10X MIC BDQ treatment was given as described above followed by CFU plating at
537 indicated time points.
538
539 **Methionine estimation**

540 Log-phase cultures of mycobacterial strains were washed with 1X PBST and transferred to 7H9
541 medium maintained at pH 7.2 or 5.5 at an OD 0.4. Cultures were allowed to grow for 6 days after
542 which they were washed with 1X PBS once followed by washing with chilled methanol. Cells
543 equivalent to OD 1 (~$3x10^8$ cells/mL) were lysed in 1 ml extraction buffer (Acetonitrile:Methanol:
544 water:: 2:2:1) by bead beating with intermittent cooling of 1 min per cycle. Lysates were clarified
545 by spinning at 13,000 rpm, 10 mins at 4°C. The clarified supernatants were filtered through 0.22-µ
546 filters and dried by speed vac to evaporate the extraction buffer. Dried pellets were resuspended in
547 methanol:water (1:1) + 0.1% formic acid and vigorously mixed. Finally, 10µL of the reconstituted
548 samples were run on Hypersil Gold C8 column (100 x 2.1mm) with 0.1% formic acid in water as
549 mobile phase A and 0.1% formic acid in acetonitrile as mobile phase B on SCIEX 6500+ QTRAP
550 and peak and retention time was matched with standard (Methionine) across all the samples. Peak
551 intensities were normalized to CFU of the respective samples.
552
553 **Total ATP estimation**
554 Cultures of *Rv-WT*, *ΔmetZ* and complement were grown at acidic pH 5.5 till OD 0.5 (mid-log phase)
555 and washed with 1X PBST. Cells were resuspended in 1000µL 1X PBST (with Protease Inhibitor
556 Cocktail) and lysed by 5 cycles: 45 seconds of bead beating with intermittent cooling on ice. Lysates
557 were passed through 0.5-µ sized filters to remove any bacterial cells or debris. 50µL of clarified
558 lysates were transferred to a 96-well plate (white, flat-bottom, SPL) and mixed (1:1) with BacTiter-
559 Glo (Promega) reaction buffer followed by incubation at 37°C for 30 minutes. 1X PBS was used as
560 blank to cancel out the background signals from the samples. Luminescence was recorded using a
561 Multimode Microplate reader (SpectraMax Pro ID3, Molecular Devices). Normalization was done
562 using total protein content of the respective samples and ATP levels were expressed as relative units
563 w.r.t. *Rv-WT* strain. For ATP estimation of BDQ treated cultures, 0.4 OD bacterial suspensions

564 (2ml) of the respective strains were treated with 2X MIC concentration of BDQ for the indicated
565 time-points and samples were prepared as described above.
566 For determination of total ATP levels upon supplementation of methionine, the bacterial strains
567 were grown to OD 0.5, washed and transferred to 7H9 (+ADS) pH 5.5 with an additional group of
568 *ΔmetZ* +Methionine. The cultures were allowed to grow for 5 days, washed with PBST and lysates
569 were prepared by bead-beating the cells. ATP estimation was performed as described above.
570

571 **Metabolic activity**

572 Auto-bioluminescent mycobacterial strains were grown till OD 0.5 (mid-log phase) and washed
573 with 1X PBST to remove the spent media. Cells were resuspended in 1X PBST and re-diluted to an
574 OD of 0.4 in media acidified to the required pH (pH 5.5). 100µL of these suspensions were added
575 to a 96-well plate (white, flat-bottom, SPL) containing 7H9 (ADS + 0.1% glycerol, pH 5.5) and
576 serially diluted (2-fold). The periphery wells were filled with sterile medium to prevent desiccation.
577 The plate was incubated at 37°C for 5 days after which 20µL of PrestoBlue (Thermo) was added to
578 each well followed by an additional incubation of 2 days to allow the development of color. After
579 2 days of incubation, luminescence read-out was taken and contents of the wells were transferred
580 to a clear bottom black plate followed by recording fluorescence of AlamarBlue at 560(ex)/
581 590(em). Ratio of Fluorescence/Luminescence was calculated to determine metabolic activity per
582 cell.
583

584 **Intracellular redox state**

585 *Rv-WT*, *ΔmetZ* and complement strains were transformed with plasmid encoding redox biosensor,
586 Mrx1-roGFP2 as described previously [47]. Cells were grown to OD 0.5 and washed with 1X PSBT
587 and resuspended in PBST in MCTs. *Rv-WT* cells in respective tubes were treated with either 100µM

588 H_2O_2 or 100μM DTT as control groups for oxidized and reduced conditions respectively. Further,
589 cells were transferred to 96-well plate (clear bottom, black wells) and excitation at 390 and 490 nm
590 while emission at 510 nm was recorded. Ratio of fluorescence at 390 nm/490 nm were compared to
591 determine intracellular redox state of the cells.
592 For determination of intracellular ROS levels upon supplementation of methionine, the bacterial
593 strains were grown to OD 0.5, washed and transferred to 7H9 (+ADS) pH 7.2 and pH 5.5 with an
594 additional group of *ΔmetZ* +Methionine. The cultures were allowed to grow for 5 days, washed with
595 PBST and resuspended in a final volume of 1ml PBST at density OD 0.5. The samples were
596 transferred to the 96-well plate (clear bottom, black wells) and excitation at 390 and 490 nm while
597 emission at 510 nm was recorded. Ratio of fluorescence at 390 nm/490 nm were compared to
598 determine intracellular redox state of the cells.
599
600 **Lipid hydroperoxidation assay**
601 Total lipids were extracted from the respective bacterial strains as described previously [48]. Briefly,
602 bacterial cells were grown to an OD 0.8-1.0 and pelleted down. Pellets were suspended in
603 methanol:chloroform (2:1), 6 ml overnight at 37°C to extract total cellular lipids. Next day, cells
604 were spun down and supernatants were collected. Supernatants having total cellular lipids were
605 further precipitated by saturating the supernatants with 0.8% KCl. The lower phase was collected
606 and dried in glass vials to evaporate the solvents and concentrate the lipids. Dried lipids were
607 resuspended in 1 ml chloroform (Sigma) and used for FOX2 assay for determining lipid
608 hydroperoxidation in the extracted lipids as described elsewhere [49]. Briefly, 200μL of the
609 concentrated lipids were mixed with 1000μL FOX2 reagent in MCTs in dark for 1hr. Samples were
610 transferred to a 96-well plate and read out at 560 nm.
611

612 **Intracellular sulfide estimation**

613 Total sulfide estimation was performed as described previously [50] [37]. Briefly, *Rv-WT*, *ΔmetZ* and
614 complement strains were grown to OD 0.5 (mid-log phase) in regular 7H9 medium supplemented
615 with OADS and 0.01% Tween 80. Cells equivalent to OD 0.5 were inoculated into 7H9 medium
616 supplemented with ADS and 0.01% tyloxapol at pH 7.2 and pH 5.5. After 4 days of incubation, the
617 cultures were pellet down and washed with 1X PBST to remove spent media. Pellets were
618 resuspended in the same media with respective pH 7.2 and 5.5 at an OD 0.4. 100µL of the cell
619 suspensions were added to 96-well plate and mixed with 100µL 2X Bismuth chloride buffer.
620 Following an incubation of 4 hours at 37°C, colorimetry was done at 405nm. The values were
621 normalized to culture OD to determine relative sulfide levels in the respective strains at two different
622 pH.

623

624 **Extracellular pH (pH_{Ex}) measurement**

625 Extracellular pH (pH_{Ex}) of the bacterial cultures was measured using pH indicator dye – Chlorophenol
626 red (CPR) as described previously [28]. Briefly, 7H9 medium supplemented with ADS and 0.01%
627 Tween 80 was used to prepare pH standards – pH 7.0, 6.5, 6.0, 5.5, 5.0, 4.5 and 4.0. To 1ml of these
628 standards, 0.004% v/v CPR was added and colorimetric read-outs at 430nm and 590nm were
629 recorded. Ratio of readouts at 430/590nm were used to prepare a pH calibration curve. For pH of
630 cultures, 250µL of bacterial cultures at indicated time points were taken and spun down at 12,000
631 rpm for 10 minutes to pellet down bacterial cells. To the supernatants, 0.004% v/v CPR was added
632 and colorimetric assay was performed as described above. Ratio of 430/590nm of cultures was used
633 to extrapolate pH_{Ex} using pH calibration curve. Fresh pH standards were prepared for each time-
634 point.

635

636 **Macrophage infection**

637 THP-1 monocytic cells were grown in RPMI medium (Lonza) supplemented with 10% fetal bovine
638 serum (FBS, Invitrogen). Further, cells were seeded at a density of $5x10^5$ cells/ well in a 12-well
639 plate (Corning) and matured for 24 hours with PMA (25ng/mL, Sigma) followed by a rest of 24
640 hours. Whenever required, cells were activated with IFN-γ (10ng/ml, Peprotech) for 16 hrs before
641 infection. Single cell suspensions of the bacterial strains (*Rv-WT*, *ΔmetZ* and complement) were
642 prepared by soft-spin method as described [43] and used for infecting resting or activated
643 macrophages at an MOI of 1. Bacteria were allowed to infect the cells for 4 hours after which,
644 extracellular bacteria were washed off by three washes with pre-warmed PBS (Gibco). At indicated
645 time points, macrophages were lysed with 1X PBS + 0.01% Triton X-100 to release intracellular
646 bacterial cells. Lysates were serially diluted and plated for bacterial enumeration.

647

648 **Confocal Microscopy**

649 THP-1 macrophages were seeded on glass coverslips in a 24-well plate ($5x10^5$ cells/well) and were
650 activated by 10ng/ml of human IFN-γ (Peprotech, USA) for 16 hours before infection. Activated
651 THP-1 cells were infected with mycobacterial strains (*Rv-WT*, *ΔmetZ* and complement) harboring
652 Live-Dead reporter plasmid [51] constitutively expressing mEmerld at an MOI of 10. After 4 hours
653 of infection, the cells were washed thrice with 1X PBS to remove the extracellular bacteria and
654 replenished with fresh media. Subsequently, after 24 hours post infection, cells were incubated with
655 50nM LysoTracker Red DND-99 (Invitogen life Technologies, CA, USA) in complete RPMI media
656 for 30 minutes at 37°C with 5% CO2 and later fixed with 4% paraformaldehyde in 1X PBS.
657 Coverslips were mounted with ProLong Diamond antifade with DAPI (Molecular Probes by Life
658 Technologies, CA, USA). Finally, slides were imaged by Olympus Confocal Laser Scanning

659 Microscope (CLSM). Later, GFP-expressing mycobacteria that colocalized with LysoTracker Red
660 was determined by analyzing the ~ 100 phagosomes and co-localization index was determined.
661

662 **Animal Infection**

663 *In-vivo* experiment in this study was performed with approval from the Institutional Animal Ethics
664 Committee (IAEC Approval No: IAEC/THSTI/165) as per guidelines laid by the Committee for the
665 Purpose of Control of Experiments on Animals (CPCEA), Government of India. Briefly, bacterial
666 suspensions of respective strains at a density of 10^8 cells/mL were prepared in normal saline and
667 guinea pigs (Duncan Hartley) were infected via aerosol route using Inhalation Exposure System
668 (Glas-Col). To determine baseline infection in all groups, a few representative animals (n=3 per
669 group) were sacrificed, followed by an evaluation of disease progression at indicated time points
670 with animals (n=5) per group; organs were harvested and bacterial burdens were determined by
671 CFU plating. Histopathological damage to the lung tissue was determined by H&E staining of lungs
672 fixed in 5% paraformaldehyde followed by granuloma scoring of the infected lung tissue.
673

674 **CRISPRi-mediated *in-vivo* fitness**

675 The experiment was performed with approval from the Institutional Animal Ethics Committee (IAEC
676 Approval No: IAEC/THSTI/196) as per guidelines laid by the Committee for the Purpose of Control
677 of Experiments on Animals (CPCEA), Government of India. Briefly, bacterial suspensions of
678 respective strains (***Rv***::NT and $\Delta Z::metB_{KD}$) at a density of $3x10^8$ cells/mL were prepared in normal
679 saline and BALB/c mice were infected via aerosol route using Inhalation Exposure System (Glas-
680 Col). To induce CRISPRi-mediated gene silencing of *metB* in $\Delta Z::metB_{KD}$ strain, doxycycline
681 (1mg/ml) was administered to mice via oral route at indicated time points [52]. NT (non-targeting
682 CRISPRi strain) was maintained with doxycycline as control which is isogenic to *Rv-WT*. Animals

683 were euthanized at indicated time points, organs (lungs and spleens) were harvested and bacterial
684 burden were determined by CFU plating.

685

686 **Bioinformatics analysis**

687 MetZ protein sequence was retrieved from Mycobrowser
688 (https://mycobrowser.epfl.ch/genes/Rv0391) and the cluster of orthologous groups analysis (COG)
689 was performed using Eggnog v5 [53]. Further, a multiple sequence alignment of the protein sequence
690 from members of *Mycobacterium* genus (*M. tuberculosis, M. bovis, M. canettii, M. marinum, M.*
691 *leprae* and *M. smegmatis*) along with gram-negative (*Pseudomonas aeruginosa*) and gram-positive
692 bacterium (*Corynebacterium glutamicum* and *Rhodococcus*) was performed using Clustal W [54] to
693 identify common domains and motifs amongst the protein sequences.

694

695 **Molecular docking and molecular dynamics (MD) simulations**

696 For system preparation, the crystal structure of putative O-succinylhomoserine sulfhydrylase of *M.*
697 *tuberculosis* was retrieved from RCSB PDB [55] (PDB-ID: 3NDN [56]). The protein has 4 chains and
698 exists in a homo-tetramer form. The receptor has a covalently bound pyridoxal-5-phosphate attached
699 to a modified lysine (K219). The substrate, O-succinyl homoserine, was retrieved from PubChem
700 (PubChemCID 439406). The substrate undergoes a sulfur transfer reaction in the presence of
701 pyridoxal-5-phosphate forming L-homocysteine which takes part in the methylation cycle. The
702 receptor protein was optimized and then minimized using the OPLS3 force field of Protein Preparation
703 Wizard module [57] of the Schrodinger suite. Next, Binding Site Identification was done using
704 AutoDock 4 [58] wherein blind docking of the substrate in the presence and absence of the cofactor to
705 identify the possible binding site was performed. Autogrid4 was used to build a 126x126x126 points

706 grid map with a spacing of 0.586 angstrom and positioned at the center of mass of the receptor protein.
707 The Lamarckian genetic algorithm was employed to generate 200 runs. On docking the substrate in the
708 presence of the cofactor, no suitable results were produced. However, docking in the absence of the
709 co-factor resulted in comparatively higher binding affinity and a larger cluster size. Focused docking
710 on the identified site was also carried out by generating a grid map of 40x40x40 units with a spacing
711 of 0.375 A and 17X20X22 as grid center coordinates. MM-GBSA of few conformers based on their
712 binding affinity and cluster size was done using Prime module [59] of the maestro. Finally, the lowest
713 energy conformations of the substrate were subsequently used for constant pH MD. Further, Constant
714 pH Molecular Dynamics Simulation (MDS) was performed with the Desmond [60] module from
715 Schrodinger suite. Both systems were protonated at pH 5.5 and 7.0, respectively, and minimized with
716 OPLS- all Atom force fields and solvated with the predefined TIP3P water solvent model. The
717 complexes were placed in the orthorhombic periodic boundary conditions to specify the shape and size
718 of the repeating unit buffered at 12 A distances. 4 Na+ and 9 Na+ ions were added to both the systems
719 respectively, to neutralize the systems. The NPT ensemble was employed for the simulation with a
720 timestep of 0.002 ps. The simulation was carried out for a total of 300 ns for each system and the
721 coordinates were saved at intervals of 20 ps to generate 15000 frames. Also, the protein was simulated
722 without the substrate at the two pH values. The post-processing of MD simulation trajectories was
723 carried out using VMD [61]. The root-mean-square-deviation and fluctuation were measured for the
724 protein, substrate and cofactor. Lastly, for thermodynamics analysis of the system we performed
725 Molecular Mechanics Generalized Born Surface Area (MM-GBSA) analysis to evaluate the MD
726 trajectories using Schrodinger software. To effectively encompass the thermodynamic properties,
727 every 500th frame was selected for MM-GBSA analysis.

728

729 **Statistics and Reproducibility**

730 The data values are represented as mean ± SEM of the replicates from two-three independent
731 experiments. Wherever applicable, the number of replicates per group have been indicated by the
732 dots. Statistical comparisons have been made with *Rv-WT* in most cases unless mentioned otherwise.
733 GraphPad Prism (ver 9.0) has been used for statistical analysis of all data with suitable statistical tests
734 mentioned with figure legend.

735

736 **Conflict of Interests**

737 The authors declare no conflict of interests

738 **Acknowledgements**

739 The authors acknowledge THSTI for infrastructural support, Department of Biotechnology,
740 Government of India for funding, the Experimental Animal Facility (and staff) for supporting animal
741 experimentations and BSL-3 facility (and staff) for conducting all *M. tuberculosis* related experiments.
742 Technical support of Mr. Surjit Yadav is duly acknowledged. We acknowledge the Multi-Omics
743 facility for LC-MS based experiments. We also duly acknowledge the receipt of plasmids and
744 constructs used in the study (as listed in Table S1).

745

746 **Funding**

747 This study was supported by the grant (No. EM/Dev/SG/212/7864/2023) from the Indian Council of
748 Medical Research (ICMR), Government of India and intramural funding by BRIC-THSTI to A.K.P.
749 and are duly acknowledged. VKN was supported by the research fellowship from ICMR (3/1/3/JRF-
750 2018/HRD-043/64467). VB is supported by the research fellowship from CSIR :
751 09/1049(11494)/2021-EMR-I. TS was supported by the research fellowship from CSIR :
752 09/1049(0036)/2019-EMR-I.

753

754 **Supplementary material**

755 1. Table S1: List of plasmids and constructs used in the study

756 2. Table S2: List of bacterial strains used in the study

757 3. Table S3: List of primers used in the study

758 4. Supplementary data

759

760 **List of relevant references:**

761

762 1. WHO, *World TB report 2022.* 2023.

763 2. Yelamanchi, S.D. and A. Surolia, *Targeting amino acid metabolism of Mycobacterium*
764 *tuberculosis for developing inhibitors to curtail its survival.* IUBMB Life, 2021. **73**(4): p. 643-
765 658.

766 3. Kim, J.M., et al., *Formyl-methionine as an N-degron of a eukaryotic N-end rule pathway.*
767 Science, 2018. **362**(6418).

768 4. Berney, M., et al., *Essential roles of methionine and S-adenosylmethionine in the autarkic*
769 *lifestyle of Mycobacterium tuberculosis.* Proc Natl Acad Sci U S A, 2015. **112**(32): p. 10008-
770 13.

771 5. Chaton, C.T., et al., *Structural analysis of mycobacterial homoserine transacetylases central*
772 *to methionine biosynthesis reveals druggable active site.* Sci Rep, 2019. **9**(1): p. 20267.

773 6. Chaudhary, D., et al., *Identification of small molecules targeting homoserine acetyl transferase*
774 *from Mycobacterium tuberculosis and Staphylococcus aureus.* Sci Rep, 2022. **12**(1): p. 13801.

775 7. Berger, B.J. and M.H. Knodel, *Characterisation of methionine adenosyltransferase from*
776 *Mycobacterium smegmatis and M. tuberculosis.* BMC Microbiol, 2003. **3**: p. 12.

777 8. Venos, E.S., et al., *Branched-chain amino acid aminotransferase and methionine formation in*
778 *Mycobacterium tuberculosis.* BMC Microbiol, 2004. **4**: p. 39.

779 9. Lee, H.S. and B.J. Hwang, *Methionine biosynthesis and its regulation in Corynebacterium*
780 *glutamicum: parallel pathways of transsulfuration and direct sulfhydrylation.* Appl Microbiol
781 Biotechnol, 2003. **62**(5-6): p. 459-67.

782 10. Hasenoehrl, E.J., et al., *Derailing the aspartate pathway of Mycobacterium tuberculosis to*
783 *eradicate persistent infection.* Nat Commun, 2019. **10**(1): p. 4215.

784 11. Smith, D.A., et al., *Characterization of auxotrophic mutants of Mycobacterium tuberculosis*
785 *and their potential as vaccine candidates.* Infect Immun, 2001. **69**(2): p. 1142-50.

786 12. Wheeler, P.R., et al., *Functional demonstration of reverse transsulfuration in the*
787 *Mycobacterium tuberculosis complex reveals that methionine is the preferred sulfur source for*
788 *pathogenic Mycobacteria.* J Biol Chem, 2005. **280**(9): p. 8069-78.

789 13. Mishra, R., et al., *Targeting redox heterogeneity to counteract drug tolerance in replicating*
790 *Mycobacterium tuberculosis.* Sci Transl Med, 2019. **11**(518).

791 14. Hatzios, S.K. and C.R. Bertozzi, *The regulation of sulfur metabolism in Mycobacterium*
792 *tuberculosis.* PLoS Pathog, 2011. **7**(7): p. e1002036.

793 15. Foglino, M., et al., *A direct sulfhydrylation pathway is used for methionine biosynthesis in*
794 *Pseudomonas aeruginosa.* Microbiology (Reading), 1995. **141 (Pt 2)**: p. 431-9.

795 16. Belfaiza, J., et al., *Direct sulfhydrylation for methionine biosynthesis in Leptospira meyeri.* J
796 Bacteriol, 1998. **180**(2): p. 250-5.

797 17. Hwang, B.J., et al., *Corynebacterium glutamicum utilizes both transsulfuration and direct*
798 *sulfhydrylation pathways for methionine biosynthesis.* J Bacteriol, 2002. **184**(5): p. 1277-86.

799 18. Cole, S.T., et al., *Deciphering the biology of Mycobacterium tuberculosis from the complete*
800 *genome sequence.* Nature, 1998. **393**(6685): p. 537-44.

801 19. Griffin, J.E., et al., *High-resolution phenotypic profiling defines genes essential for*
802 *mycobacterial growth and cholesterol catabolism.* PLoS Pathog, 2011. **7**(9): p. e1002251.

803 20. Murphy, K.C., K. Papavinasasundaram, and C.M. Sassetti, *Mycobacterial recombineering.*
804 Methods Mol Biol, 2015. **1285**: p. 177-99.

805 21. Griffin, J.E., et al., *Cholesterol catabolism by Mycobacterium tuberculosis requires*
806 *transcriptional and metabolic adaptations.* Chem Biol, 2012. **19**(2): p. 218-27.

807 22. Chang, J.C., et al., *igr Genes and Mycobacterium tuberculosis cholesterol metabolism.* J
808 Bacteriol, 2009. **191**(16): p. 5232-9.

809 23. Srivastava, M., et al., *Molecular dynamics simulation reveals the possible druggable hot-spots*
810 *of USP7.* Oncotarget, 2018. **9**(76): p. 34289-34305.

811 24. Mittal, L., et al., *Targeting cryptic-orthosteric site of PD-L1 for inhibitor identification using*
812 *structure-guided approach.* Arch Biochem Biophys, 2021. **713**: p. 109059.

813 25. Kumari, A., et al., *Deciphering the Structural Determinants Critical in Attaining the FXR*
814 *Partial Agonism.* J Phys Chem B, 2023. **127**(2): p. 465-485.

815 26. Howe, M.D., et al., *Methionine Antagonizes para-Aminosalicylic Acid Activity via Affecting*
816 *Folate Precursor Biosynthesis in Mycobacterium tuberculosis.* Front Cell Infect Microbiol,
817 2018. **8**: p. 399.

818 27. Khan, M.Z., et al., *Redox homeostasis in Mycobacterium tuberculosis is modulated by a novel*
819 *actinomycete-specific transcription factor.* EMBO J, 2021. **40**(14): p. e106111.

820 28. Gouzy, A., et al., *Growth of Mycobacterium tuberculosis at acidic pH depends on lipid*
821 *assimilation and is accompanied by reduced GAPDH activity.* Proc Natl Acad Sci U S A, 2021.
822 **118**(32).

823 29. Loewen, P.C., *Levels of glutathione in Escherichia coli.* Can J Biochem, 1979. **57**(2): p. 107-
824 11.

825 30. Akhova, A.V. and A.G. Tkachenko, *ATP/ADP alteration as a sign of the oxidative stress*
826 *development in Escherichia coli cells under antibiotic treatment.* FEMS Microbiol Lett, 2014.
827 **353**(1): p. 69-76.

828 31. Singh, S., et al., *Unraveling the role of the transcriptional regulator VirS in low pH-induced*
829 *responses of Mycobacterium tuberculosis and identification of VirS inhibitors.* J Biol Chem,
830 2019. **294**(26): p. 10055-10075.

831 32. Mehta, M., R.S. Rajmani, and A. Singh, *Mycobacterium tuberculosis WhiB3 Responds to*
832 *Vacuolar pH-induced Changes in Mycothiol Redox Potential to Modulate Phagosomal*
833 *Maturation and Virulence.* J Biol Chem, 2016. **291**(6): p. 2888-903.

834 33. Banerjee, S.K., et al., *The sensor kinase MtrB of Mycobacterium tuberculosis regulates hypoxic*
835 *survival and establishment of infection.* J Biol Chem, 2019. **294**(52): p. 19862-19876.

836 34. Choudhary, E., et al., *Deciphering the Proteomic Landscape of Mycobacterium tuberculosis in*
837 *Response to Acid and Oxidative Stresses.* ACS Omega, 2022. **7**(30): p. 26749-26766.

838 35. Rohde, K.H., et al., *Linking the transcriptional profiles and the physiological states of*
839 *Mycobacterium tuberculosis during an extended intracellular infection.* PLoS Pathog, 2012.
840 **8**(6): p. e1002769.

841 36. Saini, V., et al., *Hydrogen sulfide stimulates Mycobacterium tuberculosis respiration, growth*
842 *and pathogenesis.* Nat Commun, 2020. **11**(1): p. 557.

843 37. Kunota, T.T.R., et al., *Mycobacterium tuberculosis H2S Functions as a Sink to Modulate*
844 *Central Metabolism, Bioenergetics, and Drug Susceptibility.* Antioxidants (Basel), 2021. **10**(8).

845 38. Rahman, M.A., et al., *The Role of Host-Generated H2S in Microbial Pathogenesis: New*
846 *Perspectives on Tuberculosis.* Front Cell Infect Microbiol, 2020. **10**: p. 586923.

847 39. Rahman, M.A., et al., *Hydrogen sulfide dysregulates the immune response by suppressing*
848 *central carbon metabolism to promote tuberculosis.* Proc Natl Acad Sci U S A, 2020. **117**(12):
849 p. 6663-6674.

850 40. Brauner, A., et al., *Distinguishing between resistance, tolerance and persistence to antibiotic*
851 *treatment.* Nat Rev Microbiol, 2016. **14**(5): p. 320-30.

852 41. Quinonez, C.G., et al., *The Role of Fatty Acid Metabolism in Drug Tolerance of Mycobacterium*
853 *tuberculosis.* mBio, 2022. **13**(1): p. e0355921.

854 42. Andreu, N., et al., *Optimisation of bioluminescent reporters for use with mycobacteria.* PLoS
855 One, 2010. **5**(5): p. e10777.

856 43. Babunovic, G.H., et al., *CRISPR Interference Reveals That All-Trans-Retinoic Acid Promotes*
857 *Macrophage Control of Mycobacterium tuberculosis by Limiting Bacterial Access to*
858 *Cholesterol and Propionyl Coenzyme A.* mBio, 2022: p. e0368321.

859 44. Pandey, A.K. and C.M. Sassetti, *Mycobacterial persistence requires the utilization of host*
860 *cholesterol.* Proc Natl Acad Sci U S A, 2008. **105**(11): p. 4376-80.

861 45. Schmittgen, T.D. and K.J. Livak, *Analyzing real-time PCR data by the comparative C(T)*
862 *method.* Nat Protoc, 2008. **3**(6): p. 1101-8.

863 46. Vocat, A., et al., *Bioluminescence for assessing drug potency against nonreplicating*
864 *Mycobacterium tuberculosis.* Antimicrob Agents Chemother, 2015. **59**(7): p. 4012-9.

865 47. Bhaskar, A., et al., *Reengineering redox sensitive GFP to measure mycothiol redox potential*
866 *of Mycobacterium tuberculosis during infection.* PLoS Pathog, 2014. **10**(1): p. e1003902.

867 48. Folch, J., M. Lees, and G.H. Sloane Stanley, *A simple method for the isolation and purification*
868 *of total lipides from animal tissues.* J Biol Chem, 1957. **226**(1): p. 497-509.

869 49. Nambi, S., et al., *The Oxidative Stress Network of Mycobacterium tuberculosis Reveals*
870 *Coordination between Radical Detoxification Systems.* Cell Host Microbe, 2015. **17**(6): p. 829-
871 37.

872 50. Mishra, R., et al., *Heterogeneous Host-Pathogen Encounters Coordinate Antibiotic Resilience*
873 *in Mycobacterium tuberculosis.* Trends Microbiol, 2021. **29**(7): p. 606-620.

874 51. Cai, Y., et al., *Host immunity increases Mycobacterium tuberculosis reliance on cytochrome*
875 *bd oxidase.* PLoS Pathog, 2021. **17**(7): p. e1008911.

876 52. Tripathi, A., et al., *Mycobacterium tuberculosis requires SufT for Fe-S cluster maturation,*
877 *metabolism, and survival in vivo.* PLoS Pathog, 2022. **18**(4): p. e1010475.

878 53. Huerta-Cepas, J., et al., *eggNOG 5.0: a hierarchical, functionally and phylogenetically*
879 *annotated orthology resource based on 5090 organisms and 2502 viruses.* Nucleic Acids Res,
880 2019. **47**(D1): p. D309-D314.

881 54. Thompson, J.D., D.G. Higgins, and T.J. Gibson, *CLUSTAL W: improving the sensitivity of*
882 *progressive multiple sequence alignment through sequence weighting, position-specific gap*
883 *penalties and weight matrix choice.* Nucleic Acids Res, 1994. **22**(22): p. 4673-80.

884 55. Berman, H.M., et al., *The Protein Data Bank.* Nucleic Acids Res, 2000. **28**(1): p. 235-42.

885 56. Baugh, L., et al., *Increasing the structural coverage of tuberculosis drug targets.* Tuberculosis
886 (Edinb), 2015. **95**(2): p. 142-8.

887 57. Sastry, G.M., et al., *Protein and ligand preparation: parameters, protocols, and influence on*
888 *virtual screening enrichments.* J Comput Aided Mol Des, 2013. **27**(3): p. 221-34.

889 58. Morris, G.M., et al., *AutoDock4 and AutoDockTools4: Automated docking with selective*
890 *receptor flexibility.* J Comput Chem, 2009. **30**(16): p. 2785-91.

891 59. Jacobson, M.P., et al., *A hierarchical approach to all-atom protein loop prediction.* Proteins,
892 2004. **55**(2): p. 351-67.

60. Bowers, K.J.C., E.; Xu, H.; Dror, R. O.; Eastwood, M. P.; Gregersen, B. A.; Klepeis, J. L.; Kolossvary, I.; Moraes, M. A.; Sacerdoti, F. D.; Salmon, J. K.; Shan, Y.; Shaw, D. E., , *Scalable algorithms for molecular dynamics simulations on commodity clusters.* Proceedings of the ACM/IEEE Conference on Supercomputing (SC06), 2006.

61. Humphrey, W., A. Dalke, and K. Schulten, *VMD: visual molecular dynamics.* J Mol Graph, 1996. **14**(1): p. 33-8, 27-8.

Figures and Legends:

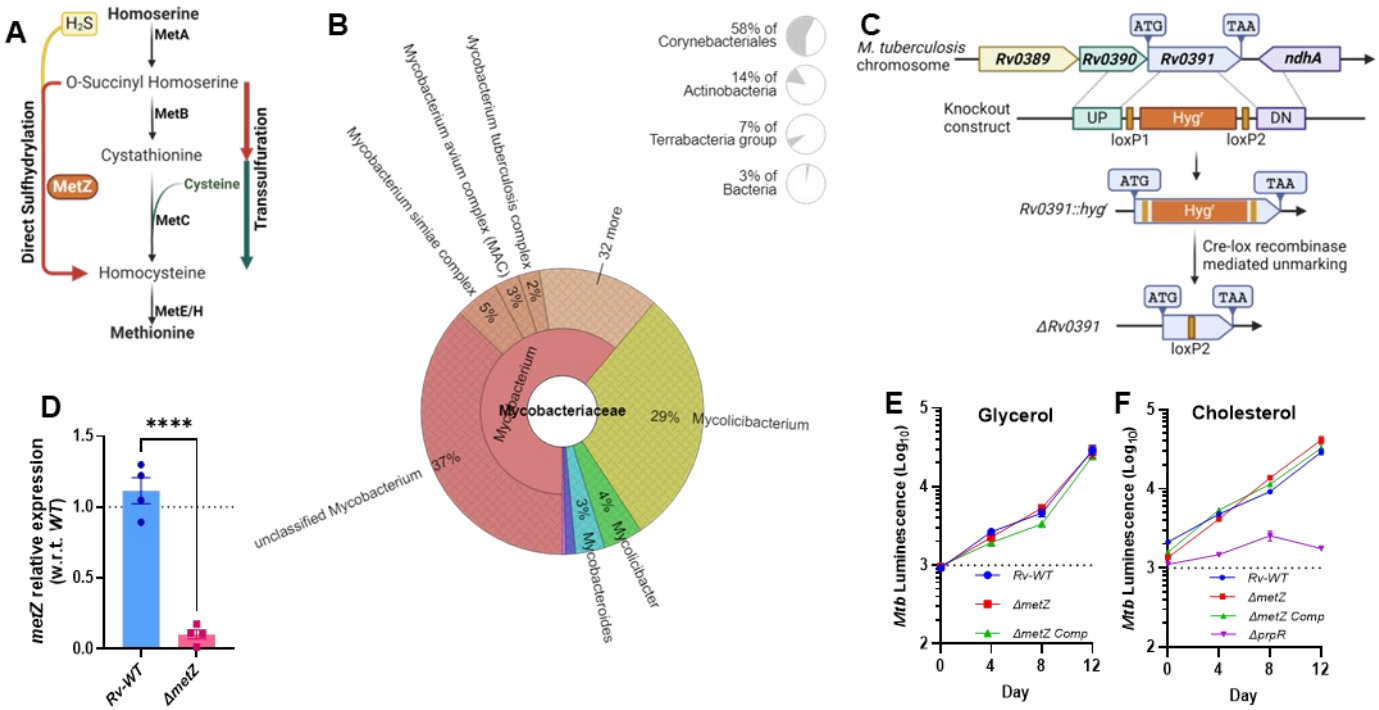

Figure 1. *metZ* is dispensable for growth in *M. tuberculosis.* (A). Methionine biosynthesis pathways in bacteria. Two alternate pathways exist in many bacterial species – transsulfuration where cysteine is used as an S-donor and direct sulfhydrylation wherein H_2S is used as an S-donor. *Rv0391* encoded MetZ is such putative O-succinyl homoserine sulfhydrylase (OSHS) involved in direct sulfhydrylation in *M. tuberculosis*. (B). Cluster of Orthologues analysis for *M. tuberculosis* MetZ (Rv0391) protein sequence with member species of ENOG502GJ5S as indicated by EggNog database. (C). Schematic for knockout generation of *ΔmetZ* in *M. tuberculosis.* (D). Confirmation of *metZ* knockout using RT-qPCR for the loss of *metZ* transcript. Growth kinetics of auto-bioluminescent *ΔmetZ* with (E) glycerol (0.1%) and (F) cholesterol (200µM) as C-source. The data summary represents means ± SEM for technical replicates from two independent experiments. Statistical comparisons were made w.r.t. *Rv-WT* for (D) using Unpaired *t*-test. ****$P<0.0001$. Comparisons not marked with statistical significance were not significant with *Rv-WT* vs *ΔmetZ* for (E) and (F).

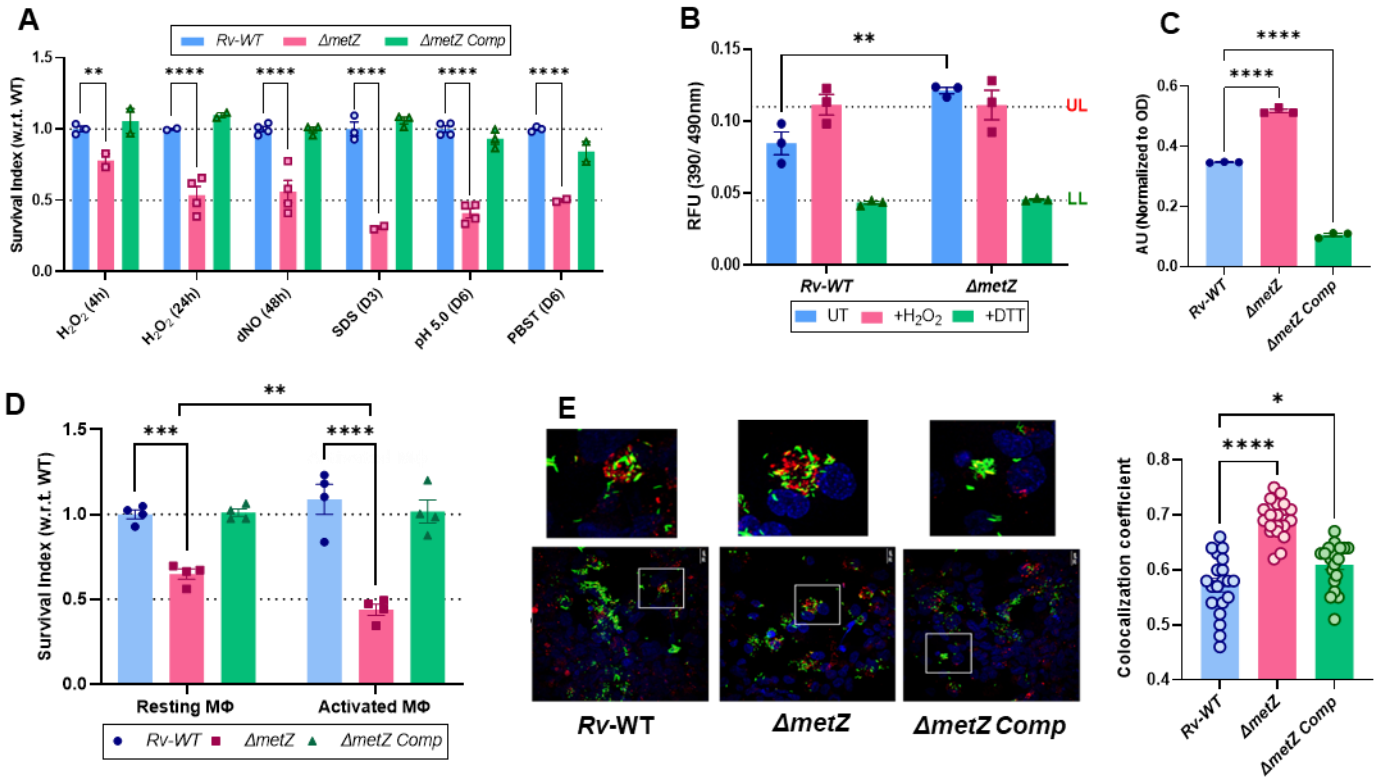

Figure 2: *metZ* deletion renders *M. tuberculosis* sensitive to physiological stressors and reduced *ex-vivo* fitness. (A). *In-vitro* stress survival assay. Mycobacterial cultures were treated with reagents mimicking host-induced stresses: H_2O_2 (Oxidative stress), DetaNO (Nitrosative stress), SDS (Surfactant stress), low pH (5.0), PSBT (nutrient starvation) *in-vitro* and survival was determined by CFU plating. (B). Intrabacterial redox state determination of *ΔmetZ* compared to *Rv-WT* using genetically encoded redox biosensor Mrx1-roGFP2. (C). Lipid hydroperoxidation levels in *ΔmetZ* compared to *Rv-WT* and complement strains using FOX2 colorimetry assay. (D). Intra-macrophage survival assay using THP-1 monocyte-derived macrophages resting or activated using IFN-γ. The survival index was determined by CFU enumeration. (E). Intracellular co-localization of GFP labelled mycobacterial strains with LysoTracker stained acidic compartments inside IFN-γ activated macrophages. Data is represented as mean ± SEM of the replicates. Comparisons for statistical significance have been made with *Rv-WT* (Control) using two-way ANOVA (Dunnett's multiple comparisons test) for (A) where **P = 0.0084, ****P<0.0001; two-way ANOVA (Sidak's multiple comparisons test) for (B) where **P = 0.0034; ordinary one-way ANOVA (Dunnett's multiple comparisons test) for (C) where ****P<0.0001; two-way ANOVA (Dunnett's multiple comparisons test) for (D) where ***P = 0.0002, ****P<0.0001; comparison of *ΔmetZ* (Resting vs. Activated macrophages) using unpaired t-test for (D) where **P = 0.0034 and ordinary one-way ANOVA for (E) where, *P = 0.0166, ****P<0.0001.

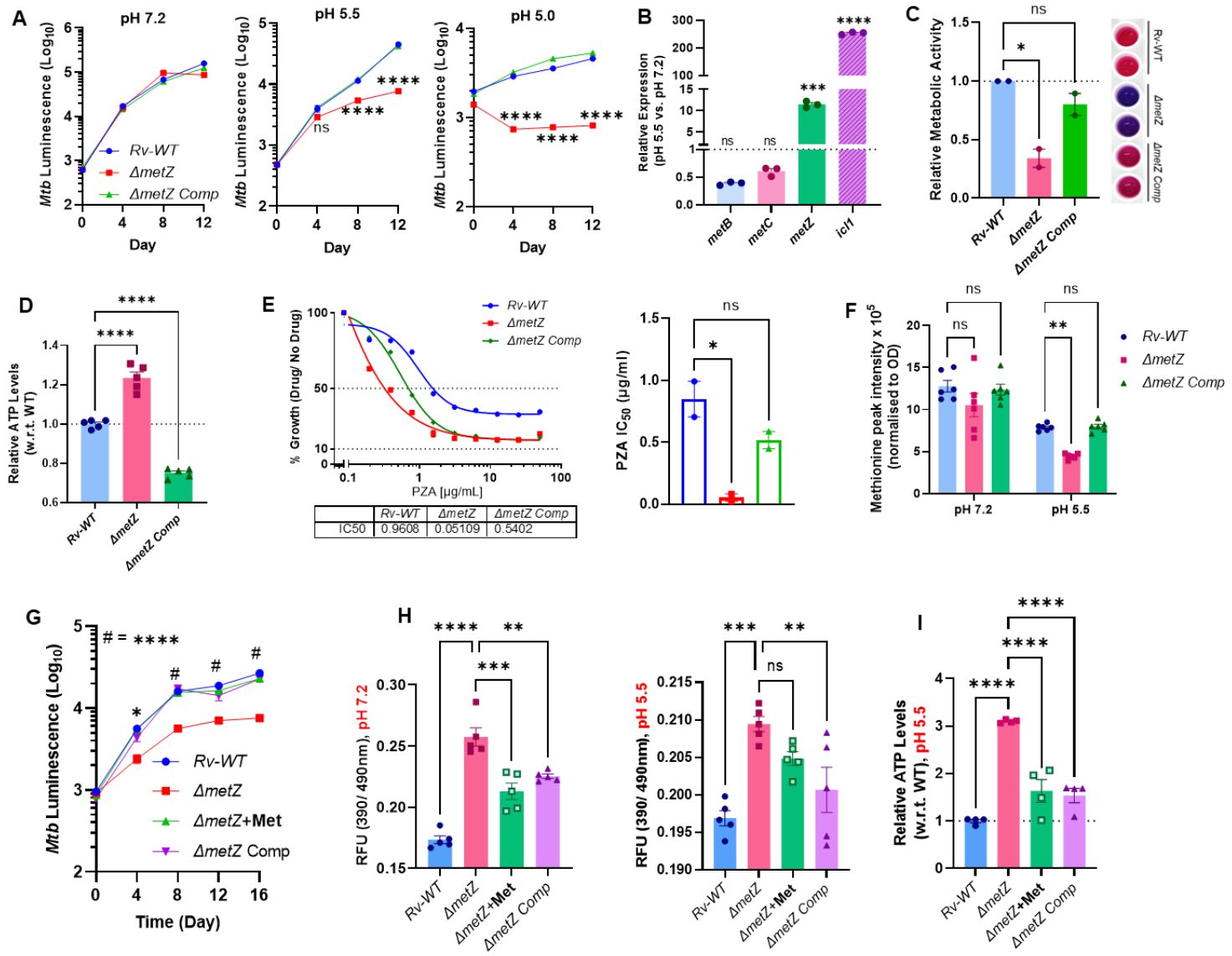

	Rv-WT	ΔmetZ	ΔmetZ Comp
IC50	0.9608	0.05109	0.5402

Figure 3: Direct sulfhydrylation pathway is essential for *M. tuberculosis* to survive at low pH. (A) *In-vitro* growth kinetics of *ΔmetZ* at various pH – 7.2, 5.5 and 5.0. (B). Expression analysis of genes involved in transsulfuration (*metB* and *metC*) and direct sulfhydrylation (*metZ*) using RT-qPCR. (C). Metabolic activity of *ΔmetZ* at acidic pH using redox dye AlamarBlue Assay. (D). Intrabacterial ATP levels estimation of *ΔmetZ* at acidic pH 5.5. (E). Pyrazinamide (PZA) sensitivity assay of *ΔmetZ* at pH 5.5. IC50 of PZA for the respective strains at acidic pH 5.5 was determined and represented as a dose-response curve. (F). Methionine estimation at pH 7.2 and pH 5.5 was performed using LC-MS. (G). Growth defect in *ΔmetZ* at pH 5.5 was rescued using exogenous methionine (Met) supplementation. (H). The intrabacterial redox state of *ΔmetZ* was determined using the Mrx1-roGFP2 redox biosensor upon supplementation with methionine (Met) at pH 7.2 and 5.5. (I). Bacterial ATP levels at pH 5.5, upon supplementation of methionine (Met). The dose-response curve for PZA was made by Non-linear regression analysis using GraphPad Prism. Data is represented as mean ± SEM of the replicates.

Comparisons for statistical significance have been made using two-way ANOVA (Dunnett's multiple comparisons test) for (A) where, ****P<0.0001, ns = non-significant; ordinary one-way ANOVA (Dunnett's multiple comparisons test) for (B) where, ***P = 0.004, ****P<0.0001, ns = non-significant; ordinary one-way ANOVA (Dunnett's multiple comparisons test) for (C) where *P = 0.011, ns = non-significant; ordinary one-way ANOVA (Dunnett's multiple comparisons test) for (D) where ****P<0.0001; ordinary one-way ANOVA (Dunnett's multiple comparisons test) for (E) where *P=0.0155, ns = non-significant; two-way ANOVA (Dunnett's multiple comparisons test) for (F) where **P = 0.0030, ns = non-significant; two-way ANOVA (Dunnett's multiple comparisons test) for (G) w.r.t. *ΔmetZ* where *P=0.0157, # = ****P<0.0001; ordinary one-way ANOVA (Dunnett's multiple comparisons test) for (H) w.r.t. *ΔmetZ* where **P<0.006, ***P<0.0004, ****P<0.0001, ns = non-significant; ordinary one-way ANOVA (Dunnett's multiple comparisons test) for (I) w.r.t. *ΔmetZ* where ****P<0.0001.

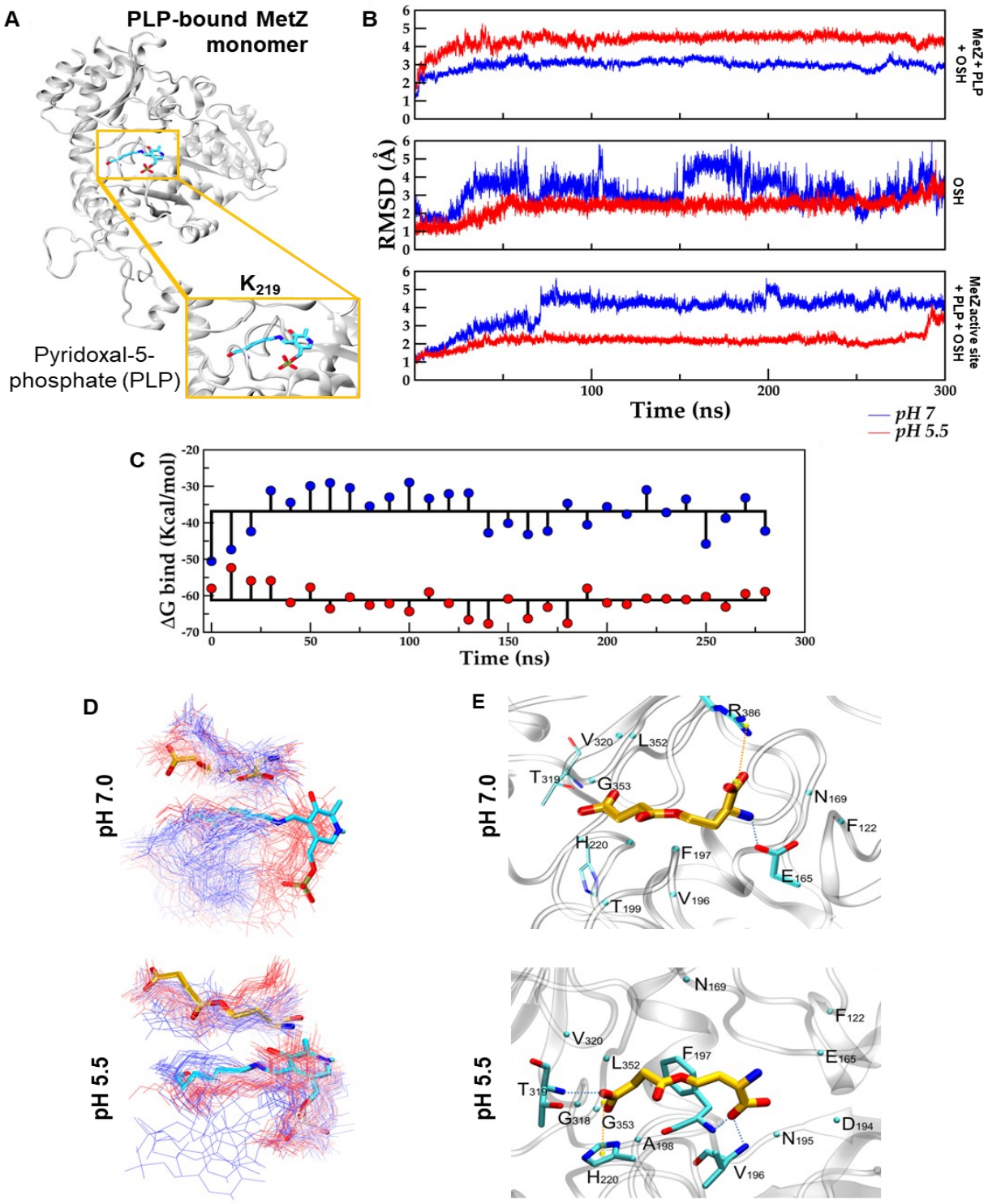

Figure 4. Molecular docking and Molecular dynamics (MD) simulations revealed enhanced stability of MetZ at acidic pH. (A). Structural representation of O-succinyl homoserine sulfhydrylase, rendered in new cartoon and colored in grey (single chain) with pyridoxal-5-phosphate in licorice and rendered atom-wise. (B). Dynamic characteristics of systems elucidated through constant pH MD simulations. The system evolution was measured via RMSD through the course of 300ns of the protein, substrate and the binding site of the substrate. Color coding is followed as the system at pH 7 (blue) and

at pH 5.5 (red). (C). The Binding Free Energy (in Kcal/mol) comparison of the complexes at pH 7 (blue) and pH 5.5 (red). (D). The dynamic changes represent the positional shifts of the substrate (orange) and co-factor (cyan) throughout the simulation, with a color gradient (time-dependent manner) from red (initial), and white (intermediate) to blue (final) at pH 7 at pH 5.5. (E). Interaction map of the substrate at pH 7 and pH 5.5. Residues lining the pocket (within 4.0 Å) are shown in licorice and colored atom-wise (C: cyan, N: blue and O: red). The residues forming hydrogen bonds (dotted line in blue) and Salt-bridges (dotted line in yellow) are shown. The Cα atom of residues involved in hydrophobic interaction are shown in beads.

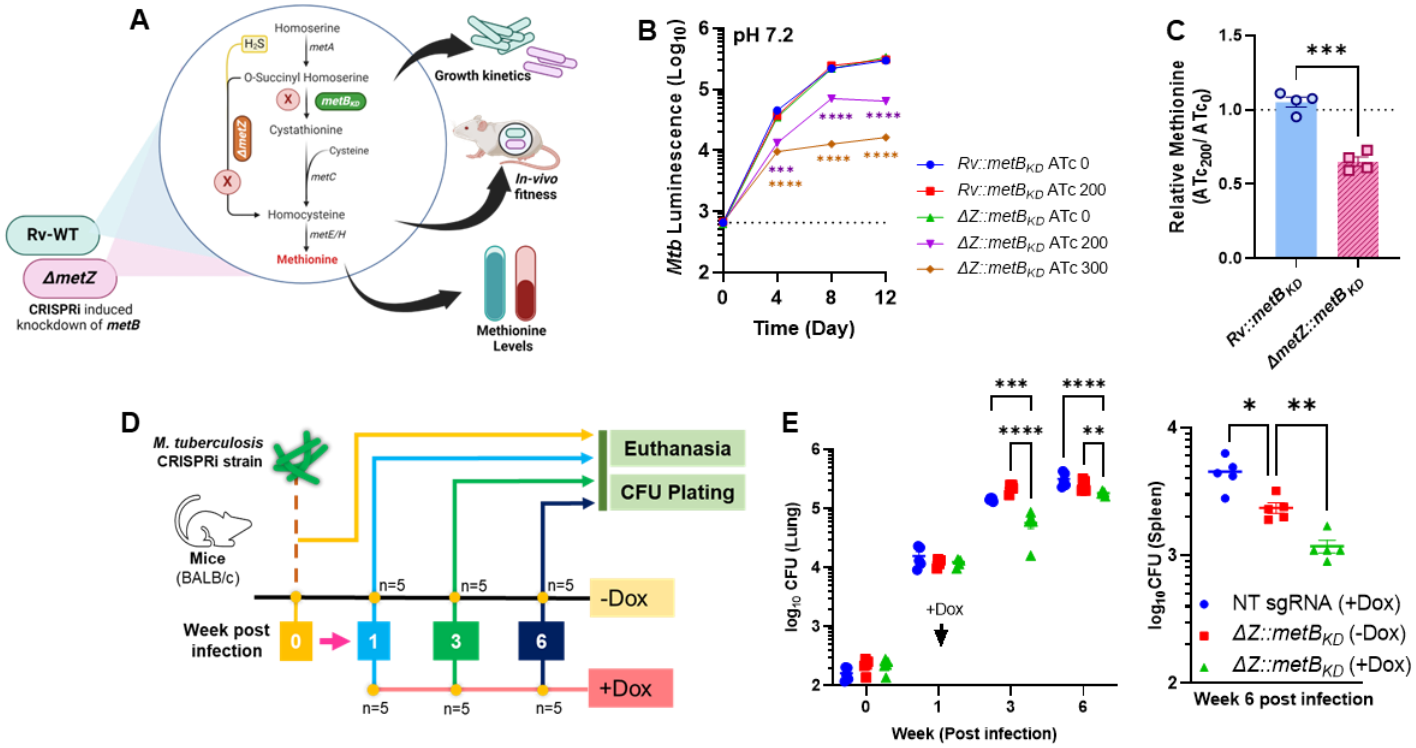

Figure 5: *metZ mediated* direct sulfhydrylation pathway is critical for methionine biosynthesis at low pH. (A). Diagrammatic representation of experimental setup to elucidate independent existence of direct sulfhydrylation pathway. CRISPRi-based knockdown of *metB* (*Rv1079*) strains was achieved in the genetic backgrounds of *Rv-WT* and *ΔmetZ* strains. Upon induction with ATc, these strains were depleted of *metB* transcripts and characterised for *in-vitro* growth kinetics, methionine levels and *in-vivo* fitness. (B). *In-vitro* growth kinetics of CRISPRi knockdown strains. (C). Relative methionine levels in CRISPRi knockdown strains either lacking *metB* (*Rv::metB*$_{KD}$) or both *metZ* and *metB (ΔZ::metB*$_{KD}$*)* by LC-MS. (D). Graphical representation of *in-vivo* fitness experiment. Mice were infected with CRISPRi knockdown of *metB* in Rv-WT and *ΔmetZ* background and orally fed with doxycycline (1mg/ml) to induce knockdown of *metB* gene in the respective strains. Bacterial burden was determined by CFU

plating in lungs and spleen homogenates. (E). and (F). The bacterial burden of mycobacterial strains lacking either *metZ*, *metB,* or both in mice lungs and spleen lysates respectively. Data is represented as mean ± SEM of replicates. Comparisons for statistical significance have been made using ordinary one-way ANOVA (Dunnett's multiple comparisons test) for (B) where ***P<0.0003, ****P<0.0001; Unpaired t-test for (C) where ***P=0.0001; Mann-Whitney Test for Spleen bacterial burden in (E) where *P=0.015, **P=0.007 and two-way ANOVA (Dunnett's multiple comparisons) for Lungs bacterial burden in (E) where **P=0.0064, ***P=0.0003 and ****P<0.0001.

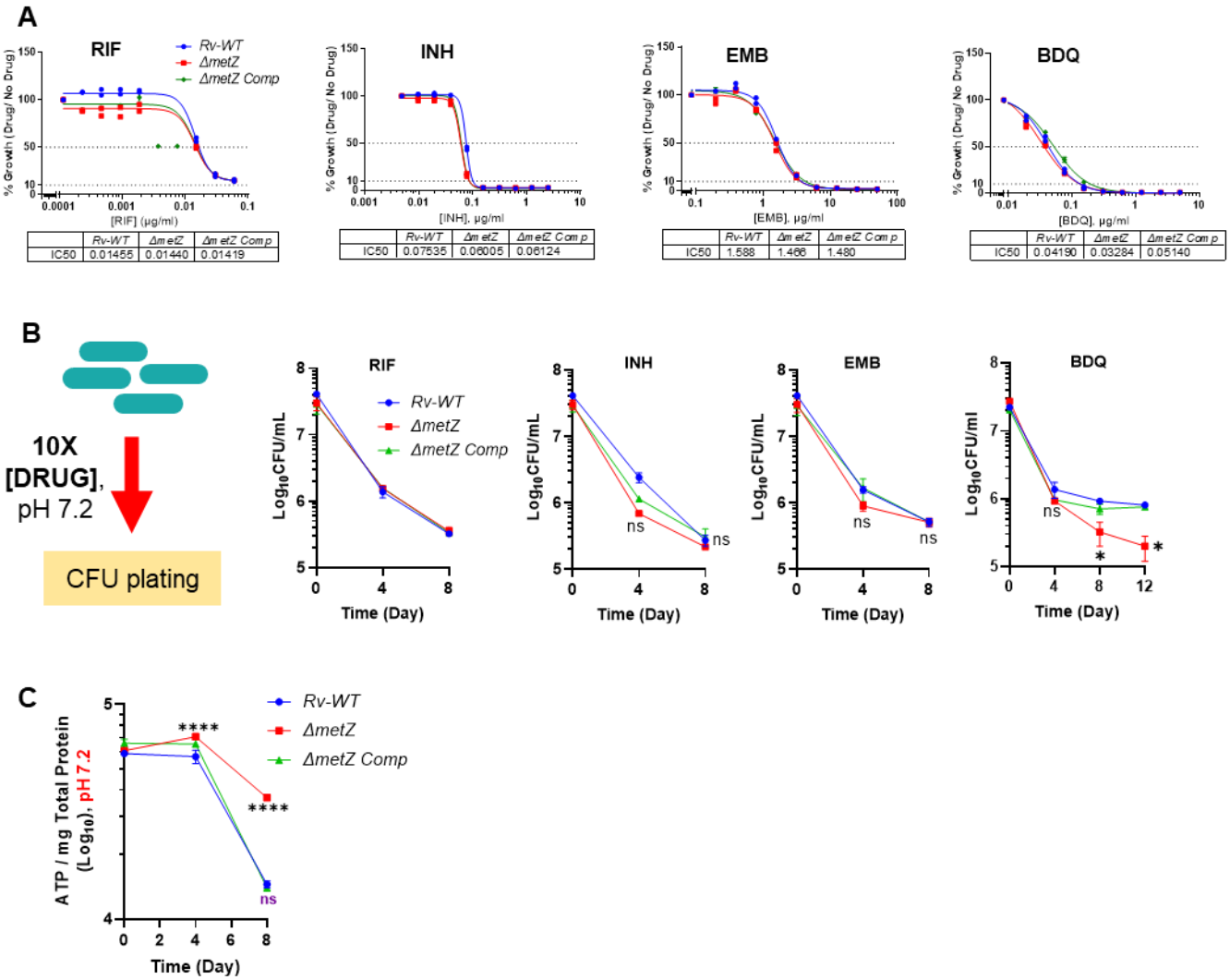

Figure 6: *metZ* is required for persister formation in the presence of BDQ. (A). Minimum Inhibitory Concentration (MIC) determination of the *ΔmetZ* in comparison to Rv-WT and Complement strains against anti-TB drugs: Rifampicin (RIF), Isoniazid (INH), Ethambutol (EMB) and Bedaquilline (BDQ) using microtiter plate assay. IC50 was determined for the drugs with the mentioned strains. (B). Kill kinetics of anti-TB drugs – RIF, INH, EMB, and BDQ at 10X MIC concentrations. Survival was determined in the form of viable bacterial count expressed as CFU. (C). Kinetics of ATP depletion post BDQ treatment. *ΔmetZ* along with Rv-WT and Complement strains were treated with 2X concentration of BDQ and ATP was estimated at indicated time points. *ΔmetZ* maintained high ATP levels. Data is represented as mean ± SEM of replicates. Comparison for statistical significance has been made using two-way ANOVA (Dunnett's Multiple Comparisons test) for (B) where *P<0.004 and ns = non-significant; two-way ANOVA (Dunnett's multiple comparisons test) for (B) where *P = 0.029, **P<0.005, ****P<0.0001 and ns, non-significant; using two-way ANOVA (Dunnett's multiple comparisons test) for (C) where ****P < 0.0001.

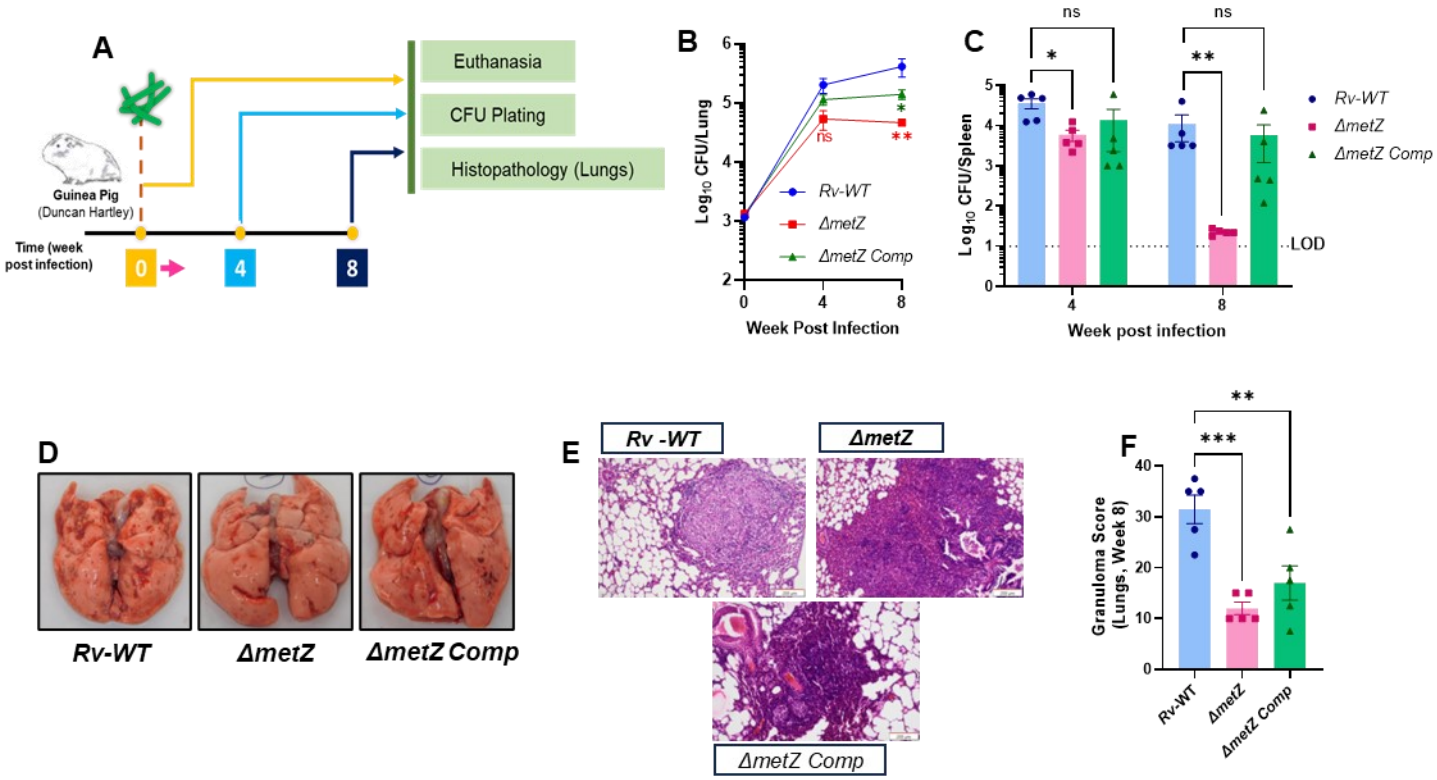

Figure 7: *metZ* is required for survival of *M. tuberculosis in-vivo*. (A). Diagrammatic representation of *in-vivo* fitness experimental set-up. Guinea pigs were infected with WT, mutant, and complement strains, and disease progression was monitored through CFU plating at indicated time points. (B). Bacterial burden in guinea pigs' lungs as determined by CFU plating of the lung homogenates of the infected animals at indicated time points. The mutant strain failed to replicate in guinea pig lungs post-week 4 of initial infection. (C). CFU burden in spleens of the infected animals revealed that the mutant could not survive inside the spleen post week 4 of infection. (D). Gross lung pathology indicates granulomatous lesions on the infected lungs at week 8-time point post initial infection. (E). H&E staining (F). Total granuloma scores of three strains in lung sections revealed significantly lesser granulomas in *ΔmetZ* infected lungs at week 8 post-infection. Data is represented as mean ± SEM of 5 replicates (animals per group). Comparison for determining statistical significance has been made using the Mann-Whitney Test for (B) and (C) where *P<0.05, **P=0.0079; ordinary one-way ANOVA (Dunnett's Multiple Comparisons test) for (F) where **P=0.004, ***P=0.0004.

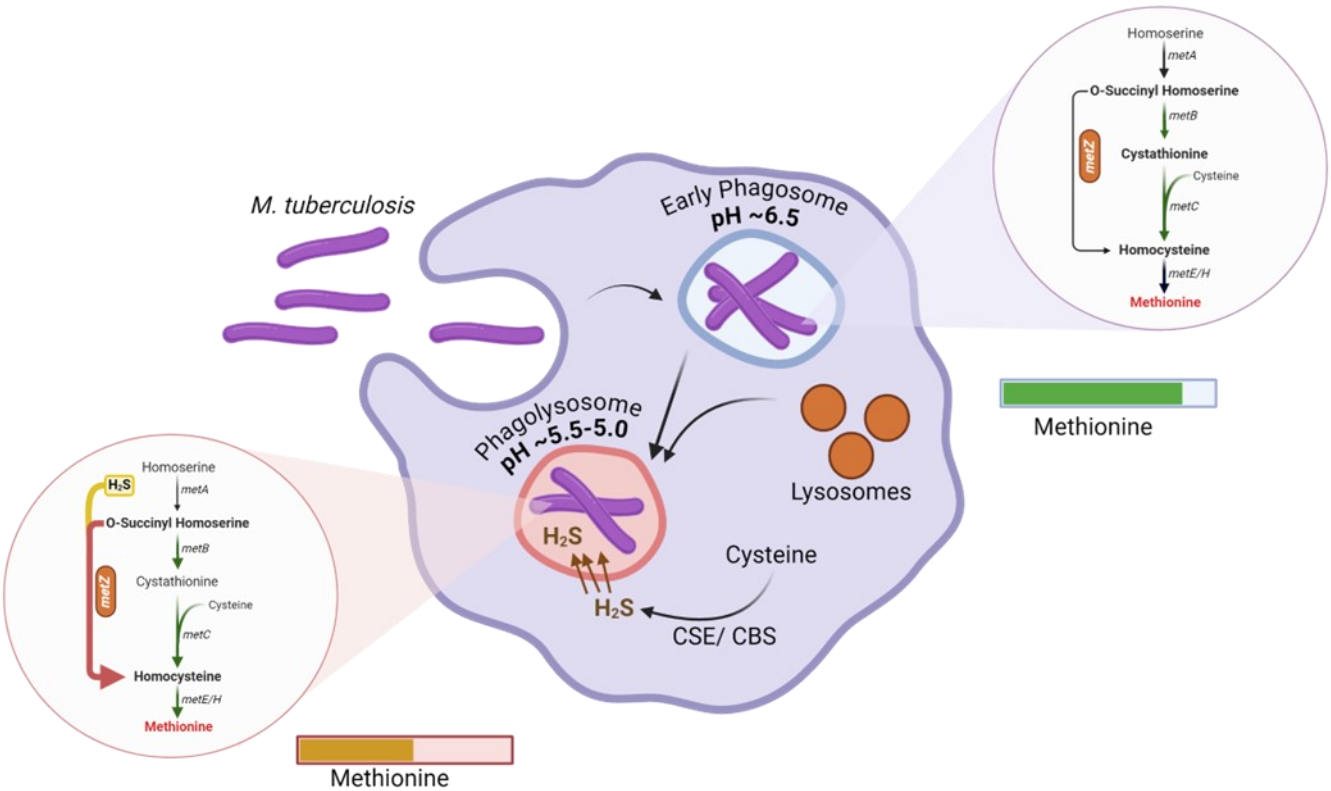

Figure 8. *MetZ-driven* direct sulfhydrylation is critical for methionine biosynthesis at low pH. When *M. tuberculosis* infects macrophage, it passes through a series of compartments starting from the phagosome where pH is essentially ~6.5 and the bacteria are replicating, with enough nutrients (including methionine). Further, as host immunity kicks in IFN-γ induced production of ROS and RNS followed by phagosome maturation leads to a drop in pH to 5.5 and beyond. Such conditions are unfavourable for *M. tuberculosis* and the host begins to quench nutrients as a means to restrict the trapped bacteria. At this stage bacteria undergo several transcriptional and metabolic changes to sustain the host-induced insults, one of these, as per our findings, includes the induction of *metZ* expression. This helps bacteria survive these stress conditions and maintain methionine levels by utilizing endogenous as well as host-generated H_2S which acts as co-substrate and S-donor for methionine biosynthesis in acidic micro-environment. This enables bacteria to maintain sufficient levels of methionine to keep adaptation going while also helping the recycling of ATP, mycothiol, at pace with its metabolic activity.